FACULTY OF SCIENCE
UNIVERSITY OF COPENHAGEN

Master's Thesis

Bacteriophage Lysis Inhibition

A Modeling Approach

Author
Ulrik Hvid ulrikhvid@gmail.com

Supervisor
Namiko Mitarai mitarai@nbi.ku.dk
Center for Models of Life
Niels Bohr Institute

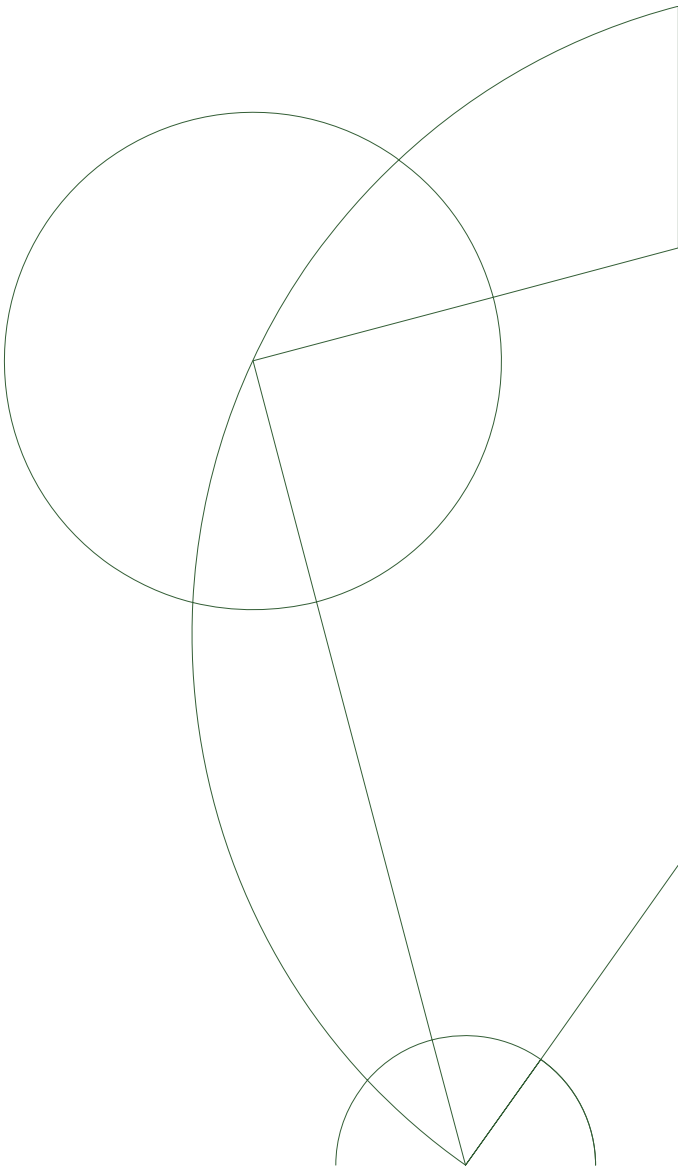

Abstract

Bacteriophage T4 is a lytic phage that employs a well-known mechanism called lysis inhibition, whereby it can delay lysis of its host in response to superinfection. Lysis inhibition is believed to constitute a significant evolutionary advantage. In this thesis, I present deterministic mean-field models which simulate interaction between phage T4 and its host, *Escherichia coli*, in various spatial configurations. My results suggest that the reproductive advantage to lysis inhibition may to some extent lie in the fact that, when a culture is widely infected by T4, keeping the culture alive may be a way of killing competing phages by letting them adsorb to already infected hosts. I present simulations of the formation of a T4 plaque, ie. the circular zone of cell destruction caused by a phage spreading in a bacterial lawn. I reproduce experimental findings which suggest that wild-type T4, which produces quite small plaques as a direct result of utilizing lysis inhibition, actually is able to spread farther in a soft agar than the small plaques would suggest. I also present simulations of phage T4 in swimming plates which may be interesting to attempt to reproduce experimentally in the future. Overall, my models support the assumption that an inducibly extended lytic cycle, such as lysis inhibition, is favorable in terms of reproduction and evolutionary competition, and that the small T4 plaques should not be taken to mean that lysis inhibition prevents the phage from effectively propagating in space.

Contents

1 Introduction

T4 is an enteric bacteriophage (phage) which takes *Escherichia coli* as its host. The strategy of infection and reproduction followed by T4 is characterized by a feature known as lysis inhibition (LIN), which involves delaying the destruction of the host cell in a situation where multiple phages infect the same cell. Several mechanisms have been suggested to explain why the LIN feature is beneficial for T4. The purpose of this thesis is to examine the ecological consequences of LIN using numerical simulation and to address the question of the adaptive benefit of LIN in a quantitative way. The modeling approach allows me to make *in silico* experiments in various spatial configurations, compare T4 to a similar phage lacking the LIN feature, and evaluate the effectiveness of different strategies in terms of number of offspring and ability to spread in space. My results suggest that, in direct competition with other phages, T4 benefits from LIN in ways that are not obvious, nor generally considered in the literature.

1.1 Introduction to phage T4

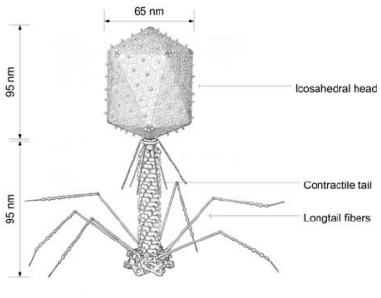

Figure 1: Schematic representation of a T4 phage. Figure by Tarik Jabrane.

A bacteriophage is a virus that infects bacteria rather than, for instance, eukaryotic cells, such as those of animals. Bacteriophages are ubiquitous in the environment, and though they cannot use human cells as hosts, they exist in large numbers as constituents of the human microbiome [1]. T4 phage belongs to the order *Caudovirales*, or tailed phages and lends its name to the subfamily known as *Tevenvirinae* - or T4-type phages. All T4-type phages share the same distinct physical appearance as T4 itself [2], with six legs, a tail, and a head (capsid) containing its genome (fig. 1). As its host, phage T4 specifically targets *Escherichia coli*, which are found in the intestines of warm-blooded animals. Enteric phages like T4 are receiving increasing recognition as playing an important role in a healthy gut ecosystem, eg. by regulating bacterial abundances [1].

In broad terms, T4's method of reproduction is similar to that of other viruses. It adsorbs to the surface of a host cell and injects its genome into its cytoplasm, at which point the host is helplessly forced to use its molecular machinery to produce offspring for the parasite. Phage T4 is characterized as a *lytic* phage, which means that, in contrast to temperate phages such as λ, the host of a T4 virion is invariably destined to be killed. The type of death that is in store for the cell is known as *lysis*, and it involves the sudden and explosive destruction of the cell, whose insides are released into the environment along with the new phage progeny.

It is well-known that, in numerical terms, bacteriophages make up the majority of organisms on the planet [3]. Indeed, with an estimated 10^{31} phages currently inhabiting the planet, they supposedly outnumber sandgrains by a factor of a trillion [4]. Despite the ubiquity of phages in nature, and in human mibrobiomes [1], and despite the groundbreaking early research, bacteriophages have been largely neglected by science for decades. However, with the looming threat of harmful bacteria developing multi-drug resistance, phage research has gained a second wind in recent years [5]. Phage T4, specifically, is being investigated as a possible treatment for intestinal diseases caused by *E. coli* [6].

1.2 Lysis inhibition

Though the destruction of the host is, by default, fairly precisely timed ($\sim$ 20 min after infection), a T4 infection will, in certain cases, last much longer, and when it does, it usually results in a larger number of offspring. This phenomenon, called lysis inhibition (LIN), happens only when the host cell is infected multiple times. In short, an *E. coli* cell infected once by T4 is set to lyse (ie. undergo lysis) after about 20 min,

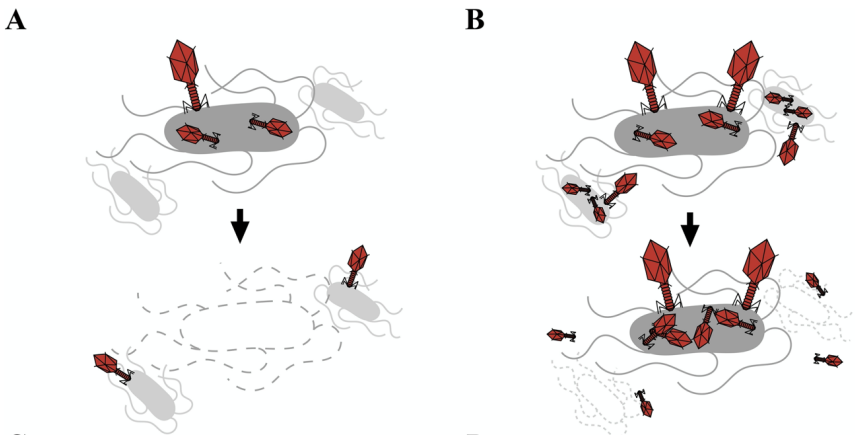

Figure 2: A graphic representation of the basic mechanism of LIN. From Hays, Seed (2020): [7]

unless it gets infected again, in which case it lyses *at some later point* - to be discussed in detail - releasing more phages than it would have after a normal lytic cycle. This is illustrated in fig. 2. The topic of this thesis is the dynamics that arise from this infection mechanism in a macroscopic system.

Research into phage T4 lysis inhibition has played an extremely important role in the history of genetics. Specifically, the identification of the so-called *r*-genes which govern LIN, was an important step in unraveling the molecular nature of the gene in general. Jim Karam sums it up: "Such seminal discoveries as the chemical nature of the gene, the existence of messenger RNA, how the genetic code is read, how genes determine protein structure, how DNA is replicated by multicomponent protein machines and many other findings that have become integral to our current understanding of basic molecular mechanism in biology have typically involved important contributions from the T4 and T4-related experimental systems." [8]

There are a few reasons why T4 and the r-genes have been so useful for the study of genetics. One is that aquiring r-mutants from a WT population is comparatively easy, as these mutations happen relatively often, with a rate of spontaneous appearance between 10^{-4} and 10^{-3} [9]. Another reason is the ease with which an r-mutant can be distinguished from a non-mutated ("wild-type", WT) phage. A typical phage experiment involves infecting a large number of bacteria spread out on a nutrient rich medium in a petri dish (a so-called bacterial lawn) with a small number of phages. The medium typically contains agar, which makes it appear solid and keeps bacteria fixed in space, while allowing smaller particles such as phages to diffuse through it. As the bacteria consume nutrients, they multiply, while the handful of added phages each infect and lyse a cell. The phage progeny spread out to neighboring cells, repeating the lytic cycle until nutrients are depleted and no more phage replication can take place. The result is that translucent circular areas called "plaques" form around the points where the first few phages found their hosts. The plaques are visible to the eye due to the fact that the remains of a destroyed cell are more transparent than was the live cell. In the case of T4, the WT plaques appear small, often ~ 1 mm in diameter, with foggy edges, whereas the mutant plaques are significantly larger and have more sharply delineated edges (fig. 3). These features are reproduced in my models.

Apart from being one of the most well-studied phage species, T4 is an organism of interest because the family of T4-like phages is very abundant in nature. Not all T4-like phages are enteric, and T4's relatives have been shown to be abundant in the oceans [11] [12]. Though it is, as far as I can tell, unclear how common the LIN feature is in phage species apart from T4 proper, as well as the lesser known T2 and T6, recent work on the molecular basis of LIN predicts that T4-like phages of various hosts will have this property [13]. The abundance of T4 and its kin has by some been ascribed specifically to the LIN feature. Paddison et.al. remark that LIN "appears to contribute significantly to the widespread occurence in nature

of these phage and to their competetive advantage," [14] while Cahill and Young write that "involving LIN allows the phage [to] make optimal use of the prey at hand." [15] Stephen Abedon has made the most thorough analysis I have seen of how evolution might select for LIN [9]. However, the proposed mechanisms by which LIN becomes a reproductive advantage have only been qualitatively characterized, with no suggestion of how to test them.

1.3 Thesis motivation

The purpose of this project is to use numerical models, designed to highlight the dynamics arising from LIN, to quantitatively explore the difference on a system containing T4 phages in interaction with bacterial prey, between a phage possessing, and one lacking, the ability to use LIN. In these models, I simplify the LIN phenomenon significantly to focus simply on the usefulness of having the binary choice: long or short lysis time, in response to information about local concentrations of phages. As I will argue, the mechanisms by which LIN benefits (or hinders) the phage should be expected to differ between different types of systems, particularly with respect to their spatial features. For this reason, I have simulated both a well-mixed or "zero-dimensional" system, as well as 2D systems where the spatial variations arise either purely from phage diffusion, or from that plus bacterial swimming.

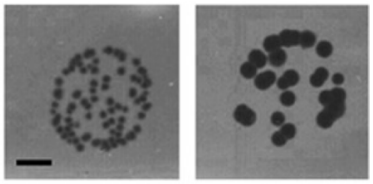

Figure 3: Plaques formed by phage T4 on a lawn of $E.coli$ B834. Scale bar: 2.5 mm. Left: T4 WT. Right: T4 ΔRI-mutant. The WT yields visibly smaller plaques with foggy edges. By comparison, the edges of the mutant-plaques are sharply outlined. From Chen, Young [10].

While much ink has been spilt on developing a model of the molecular basis of LIN, I have not seen any attempt at a quantitative model of the dynamics of LIN in a macroscopic system. A better understanding of the consequences of LIN may not only satisfy a curiosity towards the evolution of one of the most famous species of phage, but may also provide information that is useful in pharmaceutical applications of T4 [16] as well as potential future phage therapies targeting gastrointestinal diseases. Highly simplified and subject to many uncertainties, the models presented in this thesis are a first attempt at a numerical method of making testable predictions regarding the fate of an *E. coli* culture subjected to phage T4. I include a link to a Github repository containing source code for all the models in appendix A.

I believe a dialogue between simulation and experiment is a very productive way forward, since a numerical model can not only suggest explanations to previous experimental results, but also inspire experiments that one would not otherwise have considered. My supervisor, Namiko Mitarai is currently working on testing some of the predictions of this thesis in the lab.

In brief, my models support the assumption that delaying lysis in response to superinfection is a reproductive benefit to T4. In a situation where T4 competes with a similar phage which does not utilize LIN for the same host culture, this appears to be true even disregarding the increased progeny yield per host that results from LIN. The reason for this is that, when the host of a T4 virion is kept alive in an environment that is dense with the competing phage, the competitors will fruitlessly and suicidally adsorb to the already infected bacterium. In addition, when introduced into a spatially inhomogeneous environment, my models suggest that T4 is not hindered in propagating in space by using LIN. This is essentially because the diffusive front of a spreading phage population generally has low phage concentrations, meaning superinfections are extremely rare, meaning in turn that LIN will not be triggered. Thus, T4 will stay in its normal rapid-lysis mode at the interface between already infected areas and new territory, allowing it to quickly cover more ground. This is not an added feature, but an emergent result of using superinfection as the LIN trigger.

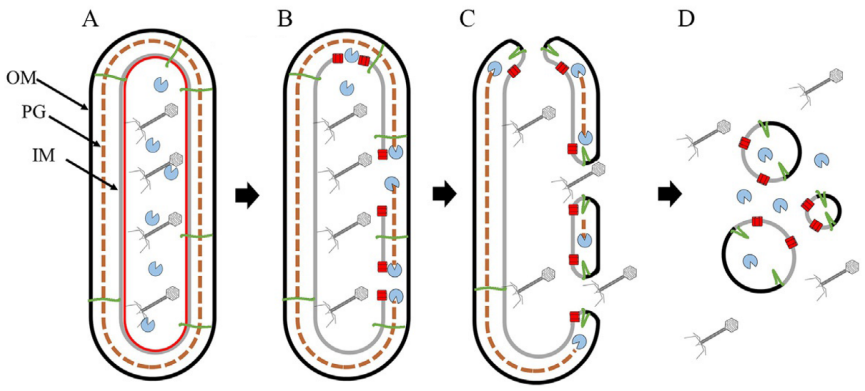

Figure 4: Schematic of the three-step model. Red: Holin. Blue: Endolysin. Green: Spanin. (A) Phages, endolysin and holin exist in the cytoplasm. Holin attaches to the inner membrane. (B) Holin activates, generating holes in the inner membrane. Endolysin starts to degrade the peptidoglycan. (C) As the peptidoglycan is degraded, spanin can now disrupt the outer membrane. (D) Lysis is complete, and both phages and lysozyme are released into the environment. From Cahill, Young (2019), [15].

2 The biology of lysis inhibition

In the following chapter, I provide an overview of the available biological knowledge of LIN, as I understand it. I first sketch the molecular biology of T4 lysis and LIN, which will be useful in making guesses about the dynamics of LIN. I will then present the LIN phenomenon as it expresses itself in different types of experimental setups. I will discuss what general dynamical rules can be extracted from experimental literature on LIN. Finally, I will present and discuss the prevailing assumptions regarding the mechanisms by which LIN becomes a useful feature in phage T4.

2.1 The three-step model of lysis

In the absence of LIN, the molecular pathway for T4 lysis is described by the "three-step model." In the following, I will sketch out this model, which roughly describes the lytic pathway not only of T4, but also a number of other species, including phage λ, which take Gram-negative bacteria as their hosts. The model is also outlined in Cahill, Young (2019) [15].

The three-step model is illustrated in fig. 4. After infection, the host's molecular machinery starts to produce not only phage progeny, but also lysozyme, a general term for the proteins that work together to disrupt the cell wall, eventually killing the cell and releasing the progeny. According to the three-step model, there are three categories of lysozymes. The *holin* protein (called T in the case of T4) attaches to the inner membrane of the host. At the end of the latent period, the holin activates to generate micron-scale holes in the inner membrane. Subsequently, an *endolysin* protein (called E in the case of T4) enters the periplasm where it degrades the peptidoglycan cell wall. This process allows the *spanin*, so named because it spans the entire periplasm and attaches to both the inner and outer membranes, to destroy the outer membrane, leading to the completion of lysis and release of the phage progeny created inside the cell. In short, the three steps of the three-step model are, 1: generation of holes in the inner membrane by holin, 2: degradation of the peptidoglycan by endolysin, and 3: disruption of the outer membrane by spanin.

2.2 The specific case of T4 and lysis inhibition

Once lysis is triggered by holin activation in the inner membrane, it happens suddenly and explosively. The timing of lysis is thus determined by the timing of the first of the three steps, after which the rest of the lytic

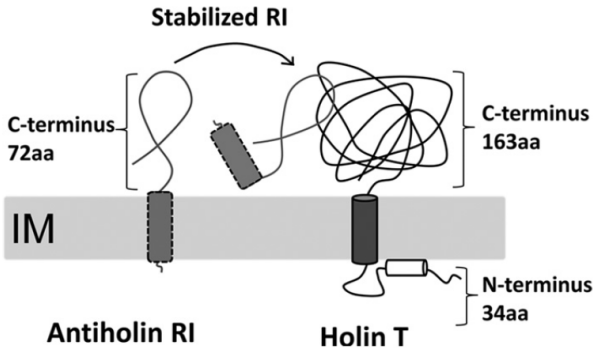

Figure 5: Schematic of the effect of the RI protein on a holin. From Chen, Young (2016) [10]

process unfolds in a matter of seconds [15]. To inhibit lysis, then, is to inhibit holin triggering. We know that this inhibition happens in response to superinfection, but what is the molecular mechanism? It is known that the proteins RI and RIII play important roles. The R here stands for "rapid lysis" precisely because mutations in the genes for these proteins lead to faster lysis [9]. In the following, I outline a molecular model of LIN, as proposed by Chen and Young (2016), [10].

RI is an example of an *antiholin*, so named because it has the ability to inhibit triggering of the holin. The protein has a transmembrane domain which is able to escape from the inner membrane, allowing RI to move from the cytoplasm into the periplasm. In the case of a single infection, RI will be quickly degraded inside the periplasm, allowing the holin to trigger and disrupt the inner membrane. However, in the LIN state, RI gets stabilized via some molecular signal conveyed by the superinfecting phage, and accumulates in the periplasm. RI can now form a complex with the periplasmic domain of the T holin, and this is what inhibits the holin triggering and resulting generation of holes in the inner membrane. Thus, the LIN-mechanism is completely reliant on the RI antiholin, and experiments show that the lysis timing of a superinfected Δri-mutant is identical to that of a singly infected WT [14].

Another protein, RIII, appears to also have an antiholin effect. Experiments have shown that a $\Delta riii$-mutant of T4 will lyse ≈ 25 min after infection, under conditions where the wild-type equivalent would enter the LIN state and not lyse, while a Δri mutant would lyse after ≈ 18 min. [10]. This could indicate, that the RI-protein in isolation, is able to inhibit lysis for some time, but that RIII is required for a stable LIN state. One model, proposed by Chen and Young [10] suggests that the stable inhibition of holin triggering requires the interaction of both RI with the periplasmic domain of T *and* of RIII with its cytoplasmic domain.

Though the role of RI and RIII are quite well-established, there is still doubt about the molecular nature of the signal that triggers LIN. It has been proposed that the signal is simply the DNA of the superinfecting phage, and a paper from 2020 has outlined a detailed model of how this signaling might come about [13].

In the rest of this thesis, I will use "r-mutant" to refer to a (simulated) phage, which does not change its lysis timing in response to superinfection. In biological terms, then, what I am simulating is a Δri-mutant.

2.3 Dynamics of lysis inhibition - Finding groundrules

In this section, I give a brief description of what is known from experiments about the dynamics of LIN and discuss what rules can be extracted from these results in terms of the timing of phage infection, lysis and reproduction. This will be the basis for the model that I build and for discussion of the relevance of its results to LIN in the real world.

Two things seem to be required for a superinfection to trigger LIN. First, the superinfecting phage must apparently belong to the T-even family (T2, T4, T6) [17]. Even if T4 performed the initial infection, infection

by T2 or T6 can still trigger LIN. Second, a superinfection will only trigger the LIN state if it takes place after a transient period, lasting 3-5 minutes, following the initial infection [10][14][15]. After that, LIN appears to be almost instantaneously inducible until the very end of the lytic cycle [14] [18]. No upper bound has been determined as to how long LIN can be maintained, and extensively LINed cells have been shown to produce more than ten times the usual ≈ 200 virions [15]. I do not include the initial 3-5 min window in my model. This is for simplicity and due to the assumption that this window is not an adapted mechanism but a necessary consequence of the fact that it takes time to complete infection of a cell. Of course, this does not mean in any case that it is necessarily unimportant to the dynamics, and it would be interesting to develop an alternative model which includes this window, to see if predictions are altered.

We know that, at least as long as we are only talking about T-even phages, the lytic pathway for T4 is solely determined by the species of the primarily infecting phage. If an *r*-mutant infects first, then a secondarily infecting WT T4 will not cause LIN any more than would another *r*-mutant. If a WT infects first, an *r*-mutant can trigger LIN just as well as another WT T4. These rules are essential to my model. They follow from the phenomenon of *superinfection exclusion*, whereby the T4 genes *imm* and *sp*, expressed by the primarily infecting phage, block the genome of a secondarily infecting phage from entering the cytoplasm [9], and thus from expression. The secondarily infecting phage is allowed to convey the LIN signal in the preiplasm, but not to let its genome be expressed by the host. Indeed, Abedon notes, "superinfection" is a misnomer in the case of T4, since only one actual infection is possible. I will use the term regardless, since it is common in the literature.

The results on the effect of superinfections on lysis timing and burst size (ie. the number of phages released from a lysing cell) are confusing. One study by Bode (1967) [18] does seem to lay down some reliable rules. His results seem to indicate that each secondary infection leads to a 5-10 min increase in total lysis time, mostly irrespective of when the secondary infection happened (as long as it happened after the transient period). However, other experiments seem to disobey this rule. As an example, in one experiment, superinfection at an MOI (multiplicity of infection, ie. number of infections to the same cell) of 10, more than 30 minutes after the initial infection, when the culture was already lysing, postponed lysis for at least 3 hours [14]. This seems to break Bode's proposed rule. One possible explanation is that the extended LIN is due to a tiny fraction of the LIN'ed culture lysing in each minute, leading to a continuous supply of phages performing further superinfections, further postponing lysis. Whether this is the correct explanation is not clear from the paper, and in any case I have not seen any other paper than Bode's which interprets LIN results in terms of such a simple rule.

The burst size of a LINed host also seems hard to predict. As an example, in one experiment, superinfection of MOI 10, 6 min after initial infection led to a doubling of burst size from 100 to 200 and an increase in lysis time from 20 to 28 min [19], while superinfection at same MOI after 10 min increased the lysis time by the same amount without leading to increase in burst size. Apart from the confusing burst size, this experiment too break seems to break Bode's proposed rule, now in the opposite direction.

There are some effects that we know contribute to this divergence in experimental results. For instance, it has been shown that the development of T4 progeny depends strongly on the physiology of the host and, by extension, on the type and abundance of available nutrients [19] [20]. Though this dependence has been quantified in some detail for the case of WT T4 without superinfection [20], a relation between host doubling rate and LINed lysis time has, to my knowledge, not been determined. This last point will become very significant in discussing the results of the spatial models.

It should be noted that, in experimental literature, the term MOI is often used in a different sense than how I will use it. Coming from an experimentalist, the statement that "a culture was infected at MOI x," means that phages were added to a bacterial culture in an amount x times larger than the number of bacteria in the culture at that time. It does not, however, follow that an average of x phages has adsorbed to each cell in the culture. This distinction is important in a modeling context. The fact that phages outnumber

cells at a given time point by, say, a factor 2, does not mean that each cell will be infected twice. The further requirement for this is, that the density of phages is large enough that a cell is likely to bump into one in the time interval between the cell's creation and division. This will be quantified later. If a culture is very dilute upon addition of phage, even if phages outnumber bacteria it may take many minutes for most of the phages to find a host, during which time the culture might grow to a point where bacteria outnumber phages. For this reason, MOI is distinguished from API (average phage input) in theoretical literature, the latter referring precisely to the ratio between total number of phages to the total number of bacteria [21]. I will use the term MOI to refer to the number of times (on average) an individual cell has actually absorbed a phage.

Another mechanism is worth mentioning which relates to the dynamics of how an infected culture as a whole eventually lyses. According to Abedon, two types of "LIN collapse" - synchronized and unsynchronized - are observable in the lab [9]. The distinction between the two, in terms of experimental observations, is in the speed with which a culture of LINed cells goes from high to low turbidity, indicating that the cells have been disintegrated. In the case of synchronized LIN collapse, it appears that the whole colony decides to lyse virtually simultaneously, whereas it happens more gradually in the unsynchronized case. Abedon proposes that this phenomenon comes from the cell wall being degraded by continued superadsorption. He notes that once the MOI reaches an excess of 50-70, extra superinfections tend to speed up, rather than inhibit, lysis. In a culture with an average MOI around 50-70, lysing cells would increase the MOI further, and this could conceivably lead to a cascade of lyses, which agrees with the macroscopic observation of synchronized LIN collapse. I am not including synchronized LIN collapse in my models, but I will refer to the concept in discussing the biological relevance of my results.

Finally, I state a few rules that do not directly relate to LIN. One characteristic of the T4 lytic cycle is that infected hosts cannot divide, nor produce many of the proteins they would normally function on. Upon infection, transcription of *E. coli*-mRNA is quickly shut off by the phage which takes control of transcription in the cell [22]. Consequently, an infected cell cannot divide. Though it probably does take up nutrients in order to create phages, I assume for simplicity that a cell stops consuming nutrients after infection. Also, I assume that an infected bacterium is still able to perform chemotaxis (swim), if the environment allows. Since infection does not happen instantaneously, it must be the case that an infected bacterium retains the ability to swim at least for some amount of time, though it would also be reasonable to assume that this ability becomes hindered at some point, given that host transcription is turned off. I have not found any experimental results on chemotaxis of T4-infected bacteria.

2.4 Evolutionary benefit of lysis inhibition

It is generally assumed in the literature on LIN that this mechanism lends a significant evolutionary benefit to phage T4. According to Ryland Young, "The logic of LIN is clear: superinfection is a signal reflecting the paucity of other host cells in the environment. In light of this environmental information, continuing the lysis pathway to liberate more progeny phage to face the same-host poor environment would obviously be suboptimal. Instead, involving LIN allows the phage makes optimal use of the prey at hand (to make more virions), extending the infection cycle until such time that superinfection signals cease." [15] Though this sounds plausible, it leaves open the question of what the phage hopes to achieve once it eventually does lyse its host. Given the superinfection signal, why is it less futile to lyse late than early? When superinfections cease, does that give the phage reason to expect that there will now be susceptible hosts in the vicinity? And does this assumption rely on the spatial dynamics of the environment, ie. will the effectiveness of LIN differ between a well-mixed planktonic environment, a distribution of biofilm clumps, or something else? Does the benefit of LIN rely on the expectation that the host will swum to a different area during the extended lysis period? Is the increased burst size an important part of the selective advantage, or is it just a

bonus, while the main advantage lies in waiting for circumstances to change?

Stephen Abedon emphasises, that the benefit relies on the fact that LIN is *inducible* rather than *constitutive* [9]. If a phage has to choose just one constitutive lysis-time, then optimizing that lysis time for highest possible basic reproductive number requires striking a balance between lysing early and lysing with a large yield of offspring, for the simple reason that it takes time to produce new phages. Things are further complicated when we imagine two competing phage species infecting a virgin culture at the same time. Conceivably, this situation could tip the optimal balance towards rapid lysis, since a phage with longer lysis time, even if it has much higher burst size, would release its progeny into an environment in which some number of the hosts are already infected by the rapid-lysis competitor. Abedon identifies two separate mechanisms that might contribute to a selective preference for an inducibly longer lysis time [9], which I present and discuss below.

Scarcity of susceptible hosts

In a situation where susceptible hosts are scarce, a released phage will spend a relatively long time seeking for a host. This decreases the cost of a longer lysis-time, because the latent period will be a relatively small fraction of the total amount of time from a phage is assembled inside a host until it infects its own host. Thus, in the tradeoff between lysing quickly and lysing profusely, the sweet spot will be shifted towards the latter. However, as Abedon also notes, scarcity of susceptible hosts does not, in and of itself, cause a superinfection signal. Scarcity is only correlated with superinfection in the specific case where the scarcity is the result of phage predation. Conversely, susceptible hosts will almost always be scarce when a cell experiences superinfection since, if a bacterium has been infected twice, there are likely very few bacteria in the immediate area that are completely uninfected. However, I would argue that, at least in the case of a well-mixed homogeneous environment, it is not clear that extending the latent period is favorable in this case, since whatever susceptible hosts remain will be infected in a very short amount of time. In well-mixed conditions, while the increased burst size does increase the probability of one offspring finding one of the remaining uninfected hosts, burst size only increases approximately linearly with the extension of lysis time, while the few remaining susceptible hosts are vanishing on an exponential time-curve in conditions where a cell is likely to be triggered into LIN.

Scarcity of susceptible hosts, I would argue, can only explain the benefit of LIN if the phage has a reason to expect that, during the time it delays lysis, there is at least some chance that the environment surrounding its host will change in the direction of greater concentration of susceptible hosts. Thus, the specific environment needs to be taken into account to explain exactly what allows the phage to expect that virions released at a later time have any chance of finding a host. Maybe the environment changes via diffusive exchange with the environment at large, or maybe the host swims to a different environment. Or, in the case of biofilms, maybe some fraction of the phages can be released into a different environment than the one the host finds itself in, ie. the phage might be released from the biofilm [9]. In any case, I would argue that mechanism number one needs to work in tandem with some sort of spatial dynamics to be effective.

Discussing the effect of spatial dynamics is complex, because phage T4 can exist in so many different types of spatial systems. A well-mixed model may represent a planktonic environment decently well. A mean-field plaque simulation, of the sort that I present in this project, where phages diffuse, but bacteria are fixed, may be representative of the inside of a biofilm, though it cannot represent the propagation of phages between biofilms. Lastly, a swimming model may also have something to say about a planktonic environment (ie. one where individual cells move freely and independently), without the assumption of homogeneity.

There might be situations where LIN represents a disadvantage. Knowing that the quintessential LIN

phenotype is a reduced plaque size, one might actually guess that LIN can in some case hinder the spatial proliferation of T4 offspring. However, my plaque model actually reproduces the experimental finding by Abedon, that the zone of infection spreads beyond the visible plaque and indeed with a speed very similar to that of an *r*-mutant.

Abundance of infected hosts and the "sink effect"

If a cell gets superinfected, the expectation for the phages released from that cell is not only that those which do find a susceptible host will take a long time to do so, but that the majority of them will adsorb to already infected hosts. Because of superinfection exclusion, then, releasing virions in the current environment will likely be fruitless. Entering the LIN state can thus be a choice to decline to release your progeny in an environment where they would be wasted via adsorption to a cell infected by the same or, perhaps, a competing species of phage. Abedon suggests that this mechanism might help explain why WT T4 has been seen to outcompete *r*-mutants in broth (liquid) cultures. [23]. Not only does the T4 avoid having its progeny attach to competitor-infected hosts by waiting until these hosts lyse, but by keeping its own host alive, it can adsorb large numbers of the competing phages that are released. The WT T4 uses its host to, as it were, sweep up the competition, before releasing its own progeny. I call this effect the "sink effect", because the LIN'ed host becomes a sink for surrounding phages.

You might say that the sink effect could just as well represent a disadvantage to the phage. If it uses its host as a sink for competing phages, how does it avoid absorbing its own kin? First of all, since LIN is triggered and prolonged by an environmental signal, it means that if a cell finds itself in the LIN state, there are probably more LINed cells in the surrounding culture, reacting to the same environmental signal. Thus, the infecting phages are effectively collaborating with each other locally, keeping their hosts alive in synchrony. Then the signal of cessation of superinfections could mean not only that the environment has become a more fruitful place to release progeny, but that keeping your host alive will no longer be effective in sweeping up competition.

Of course, the cells have to lyse eventually, and here the concept of synchronized LIN collapse becomes relevant. In light of the current discussion, it is easy to see how this effect might be the result of evolutionary adaptation, since by choosing to lyse simultaneously, the phages also avoid adsorbing to each other's hosts. I will not include synchronized LIN collapse in my models, but it would be relevant to incorporate eventually, especially if more experimental evidence on LIN collapse appears.

2.5 T4 plaque morphology

The LIN phenotype, as it appears in plaque experiments, has been observed at least as far back as 1946 [9][23]. The typical observation is that an *r*-mutant plaque is larger and more sharply delineated than that of the WT (fig. 6). In discussing the evolutionary benefits of LIN, it is worth asking whether this phenotypical difference is an indication that, in the particular artificial environment that is a soft agar, LIN actually prevents the phage from propagating as far in space as it would have without this feature.

However, experiments by Abedon indicate that the WT zone of infected bacteria is in fact much larger than the the visible plaque, and indeed similar in size to the visible plaque caused by an *r*-mutant. One of these experiments is shown in fig. 6. Here, Abedon uses chloroform vapor to selectively lyse cells that have been infected. Chloroform has the effect of degrading the plasma membrane of *E. coli*, and Abedon hypothesises that this will lead to lysis of cells that have been infected by T4, while leaving uninfected cells intact. This would agree with the three-step-model, since if endolysin and spanin are present in the periplasm, lysis will happen as soon as the inner membrane has been disrupted. As seen in fig. 6, following treatment with chloroform, the WT plaques appear similar in size to the mutant plaques. The edge of the

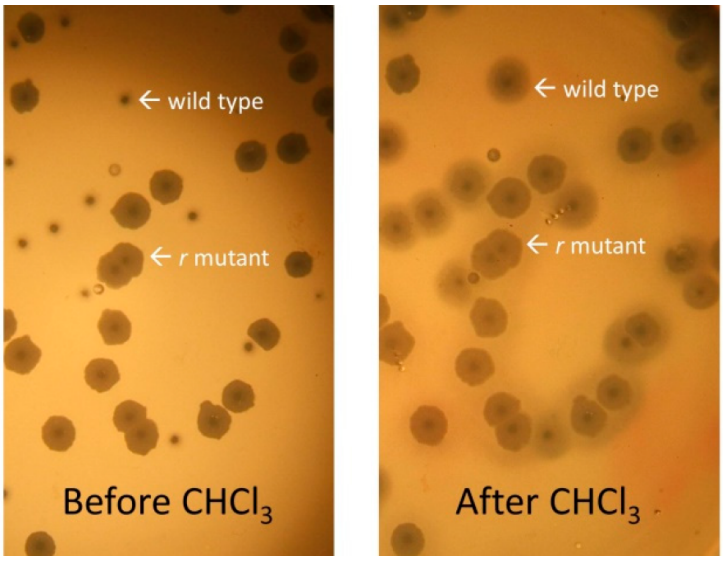

Figure 6: Crop of figure from [9] showing a plate containing both T4-WT and *r1*-mutant plaques. To the left, WT plaques are significantly smaller. To the right we see that treatment with chloroform vapor makes WT plaques appear similar in size to those of the *r*-mutant.

r-mutant plaque does not budge upon exposure to chloroform, but it does aquire a halo of its own, surrounding the sharp edge of the plaque. Abedon guesses that this halo is the result of "lysis-from-without," meaning that lysozyme released from lysed cells has partially degraded the cell envelope of some fraction of the uninfected cells in such a way that chloroform vapor is sufficient to trigger lysis.

Though fig. 6 clearly shows that some form of partial lysis has happened in the halo around the WT plaque, we cannot be sure, that this partial lysis is due to infection, let alone LIN. The partial lysis of the cells in this halo might also be due to lysis-from-without. More evidence than fig. 6 is needed to conclude that the cells led to lyse by chloroform were actually infected.

Abedon provides such evidence. Fig. 7 shows a "plaque collision", two plaques that are close enough to overlap. One plaque is WT, the other is an *ri*-mutant. The dotted circles have identical radius, representing the radius of the visible mutant plaque. The figure shows that the mutant is unable to infect cells in the area within that radius from the center of the WT plaque, except in regions closer to the center of the mutant plaque (ie. below the yellow line). In other words, *some signal*, which has the effect of preventing infection (or at least lysis) by an *r*-mutant, appears to propagate outward from the WT plaque at the same speed as the visible edge of the mutant plaque. Abedon proposes that this signal might simply be WT-infection, since superinfection exclusion means precisely that, if the the WT "got there first," adsorption by an *r*-mutant does not initialize the *r*-mutant infection cycle. Finally, a straightforward guess as to why a large part of the WT infection zone should be indistinguishable from the surrounding lawn of uninfected bacteria is that the cells in this area are in the LIN state.

One question remains, however: The expansion speed of a mutant plaque comes from the cooperation between diffusion of free phages and amplification of the phage front via phage reproduction. How is the WT infection zone able to spread with approximately the same speed as the mutant plaque if reproduction stops after some small distance? Fortunately, this question lends itself to interrogation through numerical modeling and, as we shall see, my model reproduces this behavior robustly.

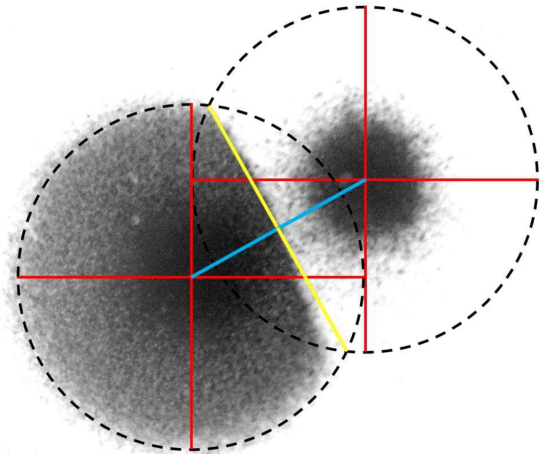

Figure 7: Close-up of adjacent plaques (a plaque collision) of a WT (right) and *ri*-mutant (left), copied from Abedon [9]. The blue line connects the centers of the plaques. The dotted circle around the WT plaque has the same radius as the *r*-mutant plaque. The yellow line connects the intersections of the circles and is at a right angle to the blue line that connects the plaque centers. The fact that the mutant plaque stops at the yellow line is an indication that some signal has spread from the center of the WT plaque at least out to the dotted circle, and that the signal has propagated with the same speed that the visible edge of the mutant plaque.

3 The models - overview

As illustrated in chapter 2.3, the dynamics of LIN seem to be quite complex, and I have not yet seen a quantitative model that clearly captures the details of the various experimental results. In exploring the adaptive benefit of LIN via modeling, then, the aim should not be to built a perfect in-silico representation of LIN dynamics, but to capture the essential choice underlying LIN mechanics: if superinfected, lyse later. Thus, my analysis will primarily be based on models that uses a binary logic, whereby a cell infected once is in the state L, and a cell infected more than once is in the state L_I. Once a cell enters the state L, is is set to lyse after an average time τ_l, releasing β phages, unless it is superinfected in the meantime, in which case it enters the state L_I. Upon entering that state, the clock starts over, and the cell is set to lyse after time $f_\tau \tau_l$, spawning $f_\beta \beta$ phages. If a cell experiences a superinfection after a fraction p of its base infection cycle, it the total lysis time will be $(f_\tau + p)\tau_l$.

For comparison, I also model rapid-lysis mutants. The model here is simpler: While an infected cell can continue absorbing free phages, this does not change its lytic fate. I generally refer to the models that do not include LIN with the number 0 and those that do with 1. The well-mixed models are thus named M0 and M1. Later I present simulations of plaque experiments, MP0 and MP1, as well as simulations of T4 in swimming plates, MS0 and MS1.

The binary structure of my LIN model is probably a significant divergence from real-world LIN dynamics. Though the exact quantitative relation is unclear, it is generally assumed that repeated superinfections lead to further delay of lysis. In light of the previous chapter's discussion of the evolutionary advantage of LIN, it cannot by any stretch be assumed that the response to continued superinfections is an unimportant component of the dynamics. Researchers have claimed that part of the evolutionary logic lies in responding to not just the onset but also the cessation of the superinfection signal [15] [14]. To me it is not obvious from literature that the cell actually does react to the cessation of the superinfection signal, but the idea certainly cannot be dismissed.

In the course of developing the models for this thesis, I have also written models that take continued superinfections into account. One of these (M3) is described in appendix B. In the report proper, I have chosen to only include M1 for the following reasons. First, as explained in chapter 2.3, I cannot see that the

experimental literature suggests any simple quantitative relationship between, on one hand, number and timing of superinfections and, on the other, timing of lysis as well as burst size. Thus, taking extra superinfections into account would still require unjustified simplifications. Second, when I modified the model to take space into account, it would give rise to difficult numerical issues, which I have been unable to resolve. Third, M1 has the benefit that the response to superinfection can be controlled in a very transparent way via the parameters f_τ and f_β (I call them the "LIN parameters"). While response to extra superinfections is not included in the model, I can rerun a simulation with varying values of the LIN parameters and thus explore the significance of various degrees of LIN. This also allows me to ask analytical questions like, what is the optimal inhibited lysis time in a given system, under the constraint that all LIN'ed cells have the same lysis-time (up to nutrient dependence).

3.1 Model reactions

The models are mean-field models that integrate ODE's (in the case of M0 and M1) or PDE's (in the case of the spatial models). Here I describe the state transitions and reactions that are represented by the equations. In the well-mixed model, these reactions of "particles" (cells, phages and nutrients) make up the entire model, while the spatial models also allow for particle movement. The model variables are the concentrations B (susceptible bacteria), P (free phages), n (nutrition), L_i (infected bacteria), and $L_{I,i}$ (LIN'ed bacteria), $i \in [1:N]$. They are represented in units ml^{-1} in the well-mixed model and $\mu\mathrm{m}^2$ in the spatial models.

First, why the index i? The simplest choice for representing the transition from infection to lysis would be to assume that lysis is a Poisson process ($\mathrm{d}L/\mathrm{d}t = ... - L/\tau$) where the duration since infection has no effect on the chance of a cell lysing in the next second. This would imply an exponential time-distribution for the lysis event, which would conflict with experimental results as they show definite sychronicity. In the absence of LIN, at least, lysis is fairly precisely timed. Thus, I want the distribution to have a peak around the chosen lysis time τ_l. However, this requires that I distinguish between particles, depending on how late they are in their lytic cycle. One way to achieve this in a mean-field model is to divide the infected state into N substates. Then we can let the transitions between subsequent states be exponentially distributed (using the term L_i/τ with $\tau \equiv \tau_l/N$). The resulting distribution in time becomes an Erlang-distribution [24]. I have chosen, rather arbitrarily $N = 10$. This gives decent synchronicity (fig. 8). Higher N demands greater computation time, and is not necessarily better, since the width of the Erlang distribution goes to zero with increasing N, while the real world presumably does allow for some variance in lysis time. Generally, I will use L to refer to the total amount of (non-LIN'ed) infected cells, ie. $L \equiv \sum_i L_i$, while L_I represents the total concentration of LIN'ed infected bacteria, $L_I \equiv \sum_i L_{I,i}$.

I take the lysis time and burst size to be functions of the amount of available nutrition, and I take the dependence from [25]:

$$\beta(n) = \beta_0 \left(r_b + (1 - r_b) \frac{g_n(n)}{g_n(n=n_o)} \right) \tag{1}$$

$$\tau_l(n) = \tau_0 / \left(r_l + (1 - r_l) \frac{g_n(n)}{g_n(n=n_0)} \right) \tag{2}$$

$$\text{with } g_n(n) = \frac{g_n^{max} n}{K_n + n} \tag{3}$$

where r_l and r_b are the ratios of maximal to minimal burst size and lysis time, respectively, and n_0 is the initial nutrient concentration. Equation 3 (Monod's law) also represents the growth rate:

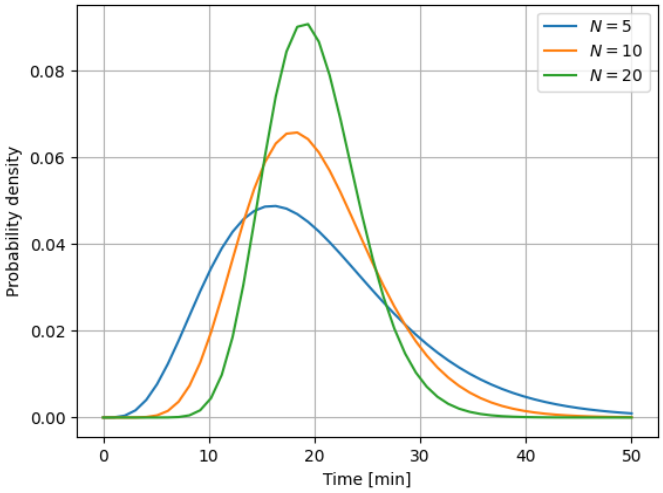

Figure 8: Erlang distributions, all with mean at 20 min, but with different values of N, representing the number of sequential Poisson processes that combine to form an Erlang distribution. The mean is conserved by fixing the time scale of each Poisson process to $\tau = 20$ min$/N$. As is apparent, the peaks do not align with the mean.

$$\frac{\mathrm{d}B}{\mathrm{d}t} = ... + \frac{g_n^{max} n}{K_n + n} B \tag{4}$$

Infection happens at the rate ηBP, ie. it is proportional to both B and P. This is a possible source of error since, in plaque as well as broth experiments, *E. coli* are known to arrange themselves spatially, for instance by grouping together in microcolonies [26]. Thus, an "ideal gas" approximation such as this is not entirely unproblematic.

η is known as the adsorption rate and has dimensions of volume pr. time. ηB can be thought of as the Poisson rate governing how soon a free phage existing in a bacterial concentration B can expect to adsorb to and infect a bacterium (and vice versa for ηP).

Nutrient depletion is represented with the term $\frac{1}{Y} g_n(n) B$. I set the depletion rate $Y = 1$, which is equivalent to choosing units such that the n represents the concentration of bacteria that will result from consuming all those nutrients. n can be thought of as the bacterial "carrying capacity" of the system. In the spatial models, where the variables are area concentrations, I use ρ to denote the "richness" of the medium, by which I mean the carrying capacity pr. unit volume. Then, the initial area carrying capacity is $n_0 = \rho \Delta a$, where Δa is the thickness of the medium. ρ is a proerty of the medium in which the bacterium finds itself, while $n0$ is a property of the particular experiment.

3.2 Parameters and initial values

Table 1 shows default parameter values as well as initial values in the simulations. None of the parameters are by any means set in stone, and below I include brief discussions of some of the most important ones.

Adsorption rate

In one study, the adsorption rate η of phage T4 was shown to vary by almost two orders of magnitude depending mainly on the growth conditions of the host [29]. Experiments performed by Hadas et. al. [19]

Parameter	Description	Default value	Source
	Well-mixed models		
g_n^{max}	Max growth rate of bacteria	$0.034\ \text{min}^{-1}$	[27] (20 min doubling time)
Y	Nutrient yield	1	Choice of unit (see n_0)
K_n	Nutrients for half-max growth rate	$n_0/5$	[27]
η	Adsorption rate	$5 \cdot 10^{-10}\text{ml/min}$	[28], [29]
τ_0	Minimum lysis-time	20 min	[19], [28]
β_0	Maximum burst size	150	[28]
f_τ	$\tau_{l,I}/\tau_l$	2-10	Varied for analysis
f_β	β_I/β	1-10	Varied for analysis
r_l	$\tau_l(n=n_0)/\tau_l(n=0)$	0.5	[25]
r_b	$\beta(n=0)/\beta(n=n_0)$	0.1	[25]
N	Number of infected states in model	10	[25]
B_0	Initial concentration of bacteria	$10^6\ \text{ml}^{-1}$	Experimental parameter
P_0	Initial concentration of phages	$10^3 - 10^8\ \text{ml}^{-1}$	Experimental parameter
n_0	Initial concentration of nutrients	$10^9\ \text{ml}^{-1}$	$Y=1 \rightarrow B_{max} = 10^9\ \text{ml}^{-1} + B_0$
	Spatial models		
ρ	Medium richness	$10^6 - 10^9\text{ml}^{-1}$	Experimental parameter
Δa	Medium thickness	0.5 mm	Experimental parameter
r_l	$\tau_l(n=n_0)/\tau_l(n=0)$	0	Necessary for frozen plaque, [27]
r_b	$\beta(n=0)/\beta(n=n_0)$	0.1	[25]
D_B	Bacterial diffusion coefficient	$800\ \mu\text{m}^2/\text{min}$	[25]
D_P	Phage diffusion coefficient	$240\ \mu\text{m}^2/\text{min}$	Value in agarose gel, [30]
D_n	Nutrient diffusion coefficient	$50000\ \mu\text{m}^2/\text{min}$	[25]
χ	Chemotactic coefficient	$20000\ \mu\text{m}^2/\text{min}$	[25]
a_+	High nutrient sensing constant	$n_0 \cdot 5$	[25]
a_-	Low nutrient sensing constant	$n_0/100$	[25]
B_0	Number of inoculated bacteria (MS)	10^6	Experimental parameter
P_0	Number of inoculated phages (MS)	10^6	Experimental parameter
n_0	Initial area concentration of nutrients	$\rho\Delta a$	

Table 1: Default parameter values and initial values. In the well-mixed models, concentrations are in units ml^{-1}, while in the spatial models they are in units μm^{-1}, and Δa is used in converting units.

suggest that this can at least in part be attributed to the fact that fast growing cells have a larger surface area so that a certain concentration of fast growing bacteria corresponds to a larger concentration of phage receptors than the same amount of slowly growing cells ("growing" here refers to culture doubling). I use a representative round number, $\eta = 5 \cdot 10^{-10}$ ml/min, which is also the value given in [28].

Burst size

Burst size, too, varies significantly. Hadas et al. have measured numbers from 12 to 152, only varying the nutrients, and I approximately cover this range with the nutrient dependence in 1 with $r_b = 0.1$. Hadas et. al were also able to get much higher values (up to 700) by restricting cell division prior to infection or triggering lysis inhibition [19]. As previously discussed, a reliable quantitative relation between multiplicity and timing of superinfection is hard to extract from the literature, so I use f_β as a free analytical parameter.

Lysis time

Hadas et al. have documented growth rate-dependent variation of lysis time between 18 and 37 min. In round numbers, I set $\tau_0 = 20$ min and $r_t = 0.5$. I have not been able to find information on the nutrient dependence of lysis time of LIN'ed cells, so in the broth models, I simply use the same factor r_t for LINed cells. This choice is not founded in biological theory or experiments, and presents some problems for my models, as I will discuss in chapter 5. Since Abedon's chloroform experiment indicates that some infected cells remain unlysed indefinitely in a WT plaque, I set $r_l = 0$ in MP. A non-zero r_t leads to a plaque which never stops expanding, which is not what is observed experimentally. $r_t = 0$ is also used in plaque simulations in [27], though they use phage λ.

4 Well-mixed models

In this chapter, I present the simplest models of my thesis, namely the broth models M0 and M1. After presenting the equations underlying the models, I present, analyze and discuss some model results. In terms of experimental biology, the models represent broth cultures, where bacteria and phages are mixed together in liquid contained in a test tube. The assumption underlying M0 and M1 is that this liquid is entirely homogeneous such that concentrations are purely functions of time. I also present a competition model M1C, which simulates both an r-mutant and a WT phage in the same culture, competing for a limited number of susceptible hosts. This model suggests a simple dynamical mechanism which might account for the evolutionary benefit of LIN.

4.1 M0 - no lysis inhibition

Below are the equations that make up the model M0 of *r*-mutants infecting a (well-mixed) broth culture. The interpretation of the terms is indicated.

$$\frac{\mathrm{d}B}{\mathrm{d}t} = \underbrace{g_n(n)\, B}_{\text{cell division}} - \underbrace{\eta\, P\, B}_{\text{infection}} \tag{5}$$

$$\frac{\mathrm{d}L_1}{\mathrm{d}t} = \underbrace{\eta\, P\, B}_{\text{infection}} - \underbrace{L_1/\tau(n)}_{\text{state progression}} \tag{6}$$

$$\frac{\mathrm{d}L_i}{\mathrm{d}t} = \underbrace{(L_{i-1} - L_i)/\tau(n)}_{\text{state progression}},\ i \in [2, N-1] \tag{7}$$

$$\frac{\mathrm{d}L_N}{\mathrm{d}t} = \underbrace{L_{N-1}/\tau(n)}_{\text{state progression}} - \underbrace{L_N/\tau(n)}_{\text{lysis}} \tag{8}$$

$$\frac{\mathrm{d}P}{\mathrm{d}t} = \underbrace{\beta(n) L_N/\tau(n)}_{\text{lysis}} - \underbrace{\eta\, P\, B_{tot}}_{\text{infection}} \tag{9}$$

$$\frac{\mathrm{d}n}{\mathrm{d}t} = - \underbrace{\frac{1}{Y} g_n(n)\, B}_{\text{cell consumption}} \tag{10}$$

$$\text{with } B_{tot} \equiv B + \textstyle\sum_{i=1}^{N} L_i \tag{11}$$

For the well-mixed simulations, I use the function *solve_ivp* under scipy.integrate. I have used the default integration method, namely fourth order Runge-Kutta (RK4(5)). Default parameter values are given in table 1.

Figure 9 shows an example run of model M0. The simulation starts with a growth phase where the bacterial culture grows exponentially. This follows from $\eta P \ll g_n$, ie. a bacterium is very unlikely to get infected before dividing. So in the early simulation, where phages are still scarce, $B = B_0 \exp(g_n t)$. Since in these particular conditions the limiting factor on growth of the culture is phage infection and not nutrient depletion, we can approximate $g_n(n) \to g_n \equiv g_n(n = n_0)$ during the entire simulation. Meanwhile, infected bacteria, as well as phages, grow superexponentially, as is apparent from the convex curves. Below I derive approximate forms of the equations for L and P which illustrate why we should expect superexponential behavior.

In the very first minutes, the L_1-curve is almost vertical, before leveling off. This leveling off is due to the negative feedback built into eq. 6, in the form of the term $-L_1/\tau$. Now, though the positive term ηPB is by no means constant in time, it does change slowly in the early simulation compared to $\tau = 2$ min

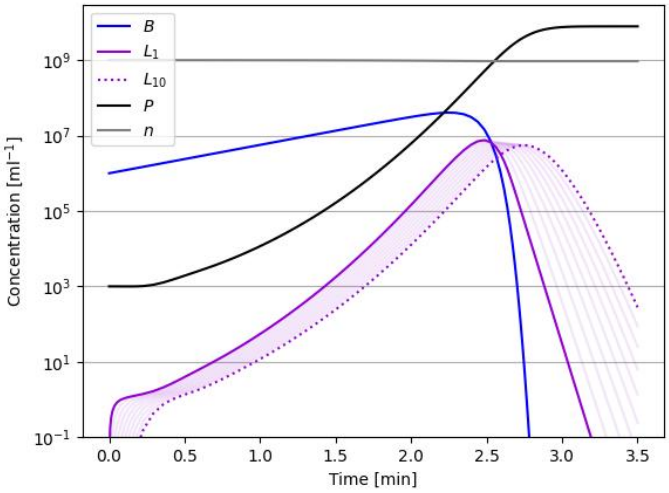

Figure 9: An example run of the broth model with r-mutant phage, M0. The thin purple lines are the intermediate infected states L_2-L_9.

(recall τ is the lysis time pr. substate, while τ_l is the total lysis time). Consequently, in the early part of the simulation, we can say that L_1 is in a quasi-steady state. This allows us to write,

$$\frac{\mathrm{d}L_1}{\mathrm{d}t} = \eta BP - L_1/\tau = 0 \implies L_1 = \tau\eta BP = \tau\eta B_0 e^{g_n t} P \tag{12}$$

Now, if we can assume perfect synchronicity in the transition from L_1 to L_N, then

$$L_N(t) = L_1(t-(N-1)\tau) = L_1(t-\phi\tau_l) = \tau\eta B_0 e^{g_n(t-\phi\tau_l)} P(t-\phi\tau_l) \tag{13}$$

with

$$\phi \equiv (N-1)/N. \tag{14}$$

This is equivalent to saying that the L_N curve is identical to the L_1 curve, just shifted in time by $(N-1)\tau$. Of course, we know that, for finite N, the L_N curve is *not* identical to the L_1 curve. The sequential Poisson distributions have the effect that sudden changes in L_1 will translate into smoothed out changes in the time-plot for L_N, according to the Erlang distribution (fig. 8). Accordingly, the sharp elbow in the early L_1-curve in fig. 9 becomes visibly rounded in the dotted L_{10}-curve. However, after the transient, there *are* no sudden changes, on the time-scale τ, as we have just assumed in eq. 12. If L_1 is approximately constant not just on the time scale $\tau = 2$ min, but also on the timescale of the width of the Erlang distribution, $\tau_l/\sqrt{N}$ which works out to ≈ 6 min in the case of fig. 9, then the assumption of perfect synchronicity, and thus eq. 13, becomes valid.

If we now insert eq. 13 into the ODE for P (eq. 9), and assume $B_{tot} \approx B$:

$$\frac{\mathrm{d}P}{\mathrm{d}t} = \eta\beta P(t-\phi\tau_l) B_0 e^{g_n\cdot(t-\phi\tau_l)} - \eta B(t)P(t) = \eta B_0(\beta P(t-\phi\tau_l)e^{g_n\cdot(t-\phi\tau_l)} - P(t)e^{g_n t}) \tag{15}$$

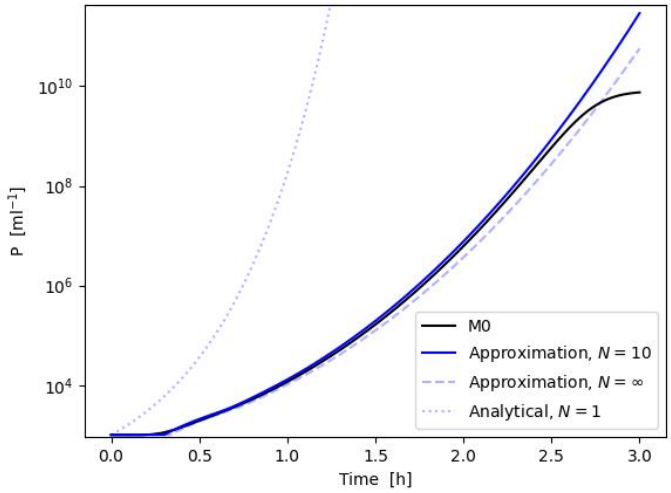

Figure 10: Numerical integration of eq. 16 together with a plot of P from the model M0.

Eq. 9 can be further simplified if it turns out that one of the terms in eq. 15 is negligible. Let us compare the two terms. On one hand, the negative term has the "advantage" that $e^{g_n t}$ is nearly twice as large as $e^{g_n(t-\phi\tau_l)}$, since the doubling time happens to be equal to the lysis time. On the other hand, the positive term has $\beta \approx 150$. So, I can throw out the negative term, if $P(t)/P(t-\phi\tau_l) \ll 150/2 = 75$. An expression for P is precisely what I lack, so I cannot show this algebraically. Looking at fig. 9, however, it seems safe to say that, in that particular simulation, P does not grow by anything like a factor 75 over 20 minutes in the early part of the simulation. Thus, I discard the negative term in eq. 15 and obtain an approximate differential equation for P:

$$\frac{\mathrm{d}P(t)}{\mathrm{d}t} = \eta\beta P(t-\phi\tau_l) B_0 e^{g_n \cdot (t-\phi\tau_l)} \tag{16}$$

in the beginning of the simulation. Eq. 16 is a delay differential equation (DDE) to which I do not know the analytical solution. If $N = 1$ (lysis as a Poisson process), the DDE becomes an ODE with a double-exponential solution:

$$P = C \cdot e^{e^{g_n t}\eta\beta B_0/g_n}\ ,\ C \equiv P_0 e^{-\eta\beta B_0/g_n} \tag{17}$$

Equation 17 massively overestimates phage growth, as seen in fig. 10, but eqs. 16 (integrated numerically in fig. 10) and 17 do share the feature of faster-than-exponential growth, as evidenced by the convex curve in fig. 10. Eq. 16 represents the general trend of P very well until after ≈ 2.5 h, which is when the assumption of exponential growth in $B(t)$ collapses entirely due to extensive phage predation. Also, fig. 10 shows that $N \to \infty \implies \phi = 1$ does not change the P curve significantly.

A few comments on the assumptions. As P grows faster than exponentially, the omission of the infection (negative) term for the ODE for P becomes less valid over time and leads us to overestimate P more and more over time. By eq. 12, as long as P grows superexponentially, so does L. This eventually means that the assumption of $B_{tot} = B$ becomes invalid.

4.2 M1 - wild-type T4 in broth culture

The model M1, represents WT T4 in a broth culture. In addition to eqs. 5 and 10 which carry over from M0, M1 consists of the following equations:

$$\frac{\mathrm{d}L_1}{\mathrm{d}t} = \underbrace{\eta\, P\, B}_{\text{infection}} - \underbrace{\eta\, P\, L_1}_{\text{superinfection}} - \underbrace{L_1/\tau(n)}_{\text{state progression}} \tag{18}$$

$$\frac{\mathrm{d}L_i}{\mathrm{d}t} = \underbrace{(L_{i-1} - L_i)/\tau(n)}_{\text{state progression}} - \underbrace{\eta\, P\, L_i}_{\text{superinfection}}\ ,\ i \in [2, N-1] \tag{19}$$

$$\frac{\mathrm{d}L_N}{\mathrm{d}t} = \underbrace{L_{N-1}/\tau(n)}_{\text{state progression}} - \underbrace{\eta\, P\, L_N}_{\text{superinfection}} - \underbrace{L_N/\tau(n)}_{\text{lysis}} \tag{20}$$

$$\frac{\mathrm{d}L_{I,1}}{\mathrm{d}t} = \underbrace{\eta\, P \sum_{i=1}^{N} L_i}_{\text{superinfection}} - \underbrace{L_{I,1}/(f_\tau \tau(n))}_{\text{state progression}} \tag{21}$$

$$\frac{\mathrm{d}L_{I,i}}{\mathrm{d}t} = \underbrace{(L_{I,i-1} - L_{I,i})/(f_\tau \tau(n))}_{\text{state progression}},\ i \in [2, N-1] \tag{22}$$

$$\frac{\mathrm{d}L_{I,N}}{\mathrm{d}t} = \underbrace{L_{I,N-1}/(f_\tau \tau(n))}_{\text{state progression}} - \underbrace{L_{I,N}/(f_\tau \tau(n))}_{\text{inhibited lysis}} \tag{23}$$

$$\frac{\mathrm{d}P}{\mathrm{d}t} = \underbrace{\beta(n) L_N/\tau(n)}_{\text{lysis}} + \underbrace{f_\beta \beta(n) L_{I,N}/(f_\tau \tau(n))}_{\text{inhibited lysis}} - \underbrace{\eta\, P\, B_{tot}}_{\text{infection}} \tag{24}$$

$$\text{with } B_{tot} \equiv B + \textstyle\sum_{i=1}^{N}(L_i + L_{I,i}) \tag{25}$$

Fig. 11 shows two example runs with, respectively, $f_\tau = f_\beta = 2, 10$. Here, I do not plot each infected substate but collapse them into $L \equiv \sum L_i$ and $L_I \equiv \sum L_{I,i}$. In both cases, the behavior is virtually identical to that in fig. 9 until approximately the end of the period of exponential growth in B. The condition for this exponential growth was that a cell is unlikely to encounter a phage before it replicates. Since the doubling time is equal to the lysis-time, this also entails that a cell is unlikely to get superinfected before it lyses. As long as no superinfections happen, recall, a WT phage is indistinguishable from an r-mutant, and so it is in M0 and M1.

In fig. 11a, as B starts to stagnate, the growth in P goes from superexponential (convex), to subexponential (concave), to superexponential, before leveling out as the remaining LINed bacteria slowly lyse. In fig. 11b, the P-curve gets not only subexponential, but actually *descends* for a little while. This wiggling sets fig. 11 apart from fig. 9. The dynamical rhythm of M1 contains two extra "beats", as it were, in the form of flips in the curvature of the P-curve on a log-plot.

The first flip is due to a sharp decline in the L curve, resulting from the depletion of susceptible hosts combined with the high rate of superinfections triggering $L_i \to L_{I,1}$. As L is declining so is the supply of new phages. The system is transitioning from a state where phages are produced by L to one where they are produced by L_I. However, the majority of L_I are in the early stages of the LIN lytic cycle, since superinfection only recently became a common occurence, so there is some latency before the next beat, which is that the P-curve becomes convex again, as L_I start lysing. Finally, P levels out, as the last L_I lyse.

Interestingly, in 11b the first beat not only leads to a more slowly growing P, but in fact leads to a decline in P. This tells us that in this case, where superinfected cells stick around for a very long time, they will superadsorb a significant number of phages before lysing. This point becomes significant later when we look at competition simulations in 0D.

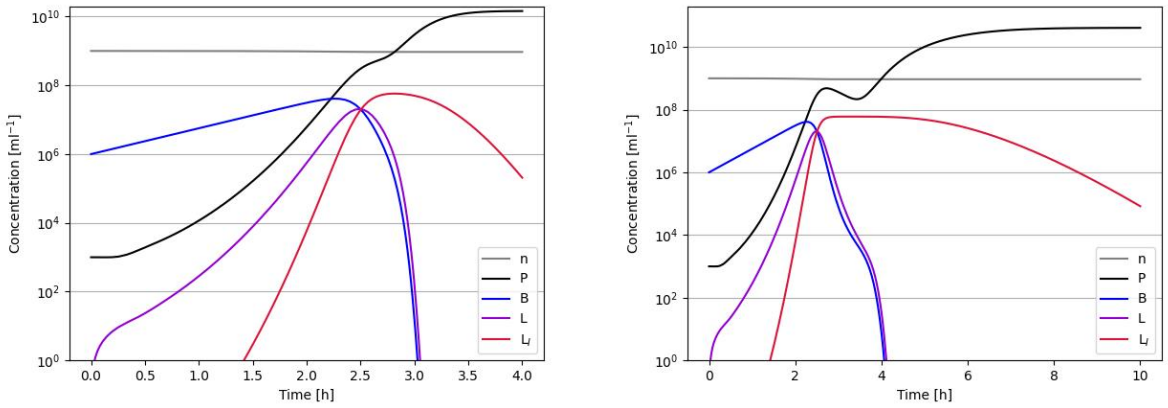

(a) (b)

Figure 11: Example runs of model M1. I use parameters according to table 1 as well as (a): $f_\tau = f_\beta = 2$. (b) $f_\tau = f_\beta = 10$.

4.3 M1C - Competition in broth culture

The model M1C simulates competition between a WT T4 and an r-mutant in a well-mixed environment. Here, concentrations of r-mutant phages and infected are denoted by the variable P_r and $L_{r,i}$, respectively, while WT virions and their hosts keep the names P and L_i. Every type of cell can absorb either type of phage. If the absorbing cell belongs to L_i, it will enter the first LIN substate, $L_{I,1}$. If it belongs to $L_{I,i}$ or $L_{r,i}$, the superinfection has no effect on the cell. L_i and $L_{r,i}$ have the same $\tau(n)$ and $\beta(n)$. The ODE's are,

$$\frac{\mathrm{d}B}{\mathrm{d}t} = \underbrace{g_n(n)\ B}_{\text{cell division}} - \underbrace{\eta\ (P + P_r)\ B}_{\text{infection}} \tag{26}$$

$$\frac{\mathrm{d}L_1}{\mathrm{d}t} = \underbrace{\eta\ P\ B}_{\text{infection}} - \underbrace{\eta\ (P + P_r)\ L_1}_{\text{superinfection}} - \underbrace{L_1/\tau(n)}_{\text{state progression}} \tag{27}$$

$$\frac{\mathrm{d}L_i}{\mathrm{d}t} = \underbrace{(L_{i-1} - L_i)/\tau(n)}_{\text{state progression}} - \underbrace{\eta\ (P + P_r)\ L_i}_{\text{superinfection}},\ i \in [2, N-1] \tag{28}$$

$$\frac{\mathrm{d}L_N}{\mathrm{d}t} = \underbrace{L_{N-1}/\tau(n)}_{\text{state progression}} - \underbrace{\eta\ (P + P_r)\ L_N}_{\text{superinfection}} - \underbrace{L_N/\tau(n)}_{\text{lysis}} \tag{29}$$

$$\frac{\mathrm{d}L_{I,1}}{\mathrm{d}t} = \underbrace{\eta\ (P + P_r)\ \sum_{i=1}^{N} L_i}_{\text{superinfection}} - \underbrace{L_{I,1}/(f_\tau \tau(n))}_{\text{state progression}} \tag{30}$$

$$\frac{\mathrm{d}L_{I,i}}{\mathrm{d}t} = \underbrace{(L_{I,i-1} - L_{I,i})/(f_\tau \tau(n))}_{\text{state progression}},\ i \in [2, N-1] \tag{31}$$

$$\frac{\mathrm{d}L_{I,N}}{\mathrm{d}t} = \underbrace{L_{I,N-1}/(f_\tau \tau(n))}_{\text{state progression}} - \underbrace{L_{I,N}/(f_\tau \tau(n))}_{\text{inhibited lysis}} \tag{32}$$

$$\frac{\mathrm{d}L_{r,1}}{\mathrm{d}t} = \underbrace{\eta\ P_r\ B}_{\text{infection}} - \underbrace{L_{r,1}/\tau(n)}_{\text{state progression}} \tag{33}$$

$$\frac{\mathrm{d}L_{r,i}}{\mathrm{d}t} = \underbrace{(L_{r,i-1} - L_{r,i})/\tau(n)}_{\text{state progression}},\ i \in [2, N-1] \tag{34}$$

$$\frac{\mathrm{d}L_{r,N}}{\mathrm{d}t} = \underbrace{L_{r,N-1}/\tau(n)}_{\text{state progression}} - \underbrace{L_{r,N}/\tau(n)}_{\text{lysis}} \tag{35}$$

$$\frac{\mathrm{d}P}{\mathrm{d}t} = \underbrace{\beta(n) L_N/\tau(n)}_{\text{lysis}} + \underbrace{f_\beta \beta(n) L_{I,N}/(f_\tau \tau(n))}_{\text{inhibited lysis}} - \underbrace{\eta\ P\ B_{tot}}_{\text{infection}} \tag{36}$$

$$\frac{\mathrm{d}P_r}{\mathrm{d}t} = \underbrace{\beta(n) L_{r,N}/\tau(n)}_{\text{lysis}} - \underbrace{\eta\ P_r\ B_{tot}}_{\text{infection}} \tag{37}$$

$$\text{with } B_{tot} \equiv B + \textstyle\sum_{i=1}^{N} (L_i + L_{I,i} + L_{r,i}) \tag{38}$$

4.4 Results of competition simulations

To explore the fitness advantage of LIN, I make simulations where I pit a wild-type T4 against an *r*-mutant, which cannot perform LIN. Figure 12 shows an example simulation. We see that the two phages display virtually identical behavior in the early stages of the simulation, just as we saw in the separate simulations of WT and *r*-mutant (figs. 9, 11). As P and P_r diverge, the *r*-mutant appears to win, as its hosts are lysing at the same rate as before, while some of the WT-hosts are kept alive in the LIN-state. However, once the inhibited cells start to lyse with twice the burst size, the WT overtakes the mutant and ends up being more abundant than its competitor.

The WT is running a risk here. When declining to lyse as the bacterial culture starts to decline, it allows the mutant to infect the majority of the remaining population. In other words, since $P_r > P$ in the period of culture collapse, and $P_r \approx P$ prior to that, the mutant aquires more hosts in total than does the WT. It would seem that the WT's victory is dependent on the increased burst size to compensate for this initial

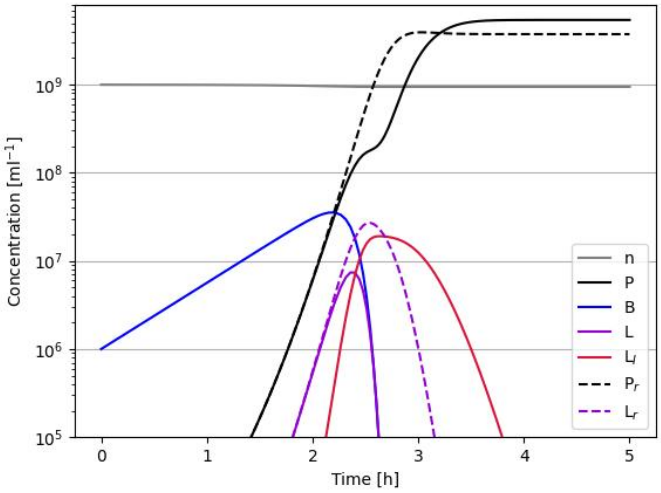

Figure 12: Competition simulation in broth. $f_\tau = f_\beta = 2$. $B_0 = 10^6 \text{ml}^{-1}$,$P_0 = 10^3 \text{ml}^{-1}$.

disadvantage.

However, this is not the whole story. It turns out that, in this model, the WT will in many cases win even without the benefit of increased burst size. This is exemplified by an extreme case in figure 13, where the LIN'ed lysis time is very high ($f_\tau = 10$) while the LIN'ed hosts lyse with the same burst size as the non-LIN'ed ($f_\beta = 1$). While the mutant initially wins by more than an order of magnitude, the WT ends up taking the victory. The explanation lies in the model feature that infections happening after the one that initialized LIN have no effect apart from inactivating the infecting phage (superinfection exclusion). After the mutant phages peak, they are now coexisting with a high concentration of LIN'ed bacteria, to which they helplessly adsorb. This is the reason for the decline in P_r following the peak. By the time the LIN'ed hosts lyse, the population of free mutant phages has been significantly decimated, and the WT ends up outnumbering the competition, even though it ends up at a lower concentration than the mutant had previously reached. In a sense, the WT phage uses its host to "vacuum up" the competition, before destroying it. I will call this the "sink effect" since the LIN'ed bacteria act as sinks for free phages.

In figure 13, the sink effect is very pronounced, because the extended lysis time means that the WT has a long time to sweep up the competition. What would it take, in terms of the LIN-parameters, for the mutant to win due to the advantage it gets from infecting more hosts? Figure 14a shows that, at least for these initial concentrations, the WT wins with virtually any combination of f_τ and f_β. It also shows, that the WT's margin of victory increases monotonically with both parameters. The exception to this is the upper left corner. The explanation for this second peak is that, with small f_τ and large f_β, the WT can gain the upper hand even during the period of exponential growth of B, because the tiny number of LIN'ed bacteria in this period burst with such huge size. Since the logic of LIN lies in the option of extending lysis time - and as a necessary result, aquiring a larger burst size - and not in getting a huge burst size for free, the upper left corners in figure 14 have no biological relevance.

The gradient in figure 14a points approximately along the diagonal $f_\tau = f_\beta$, indicating that increased lysis time and burst size are equally useful in beating the competition. Furthermore, this diagonal approximately represents the biologically "realistic" part of phase space, insofar as phage progeny are produced with a constant rate after superinfection.

The results of figure 14 are strongly dependent on the initial concentrations in the simulation. First of all, this discussion assumes that the initial conditions allow for a period of exponential bacterial growth

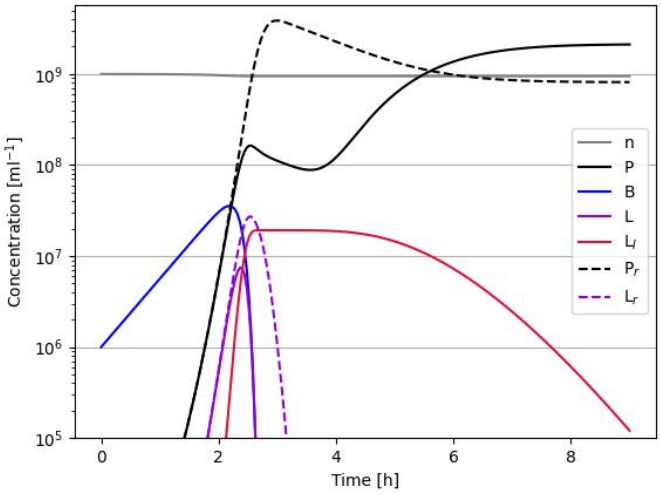

Figure 13: Competition simulation in broth. $f_\tau = 10,\ f_\beta = 1$. $B_0 = 10^6 \text{ml}^{-1}$,$P_0 = 10^3 \text{ml}^{-1}$.

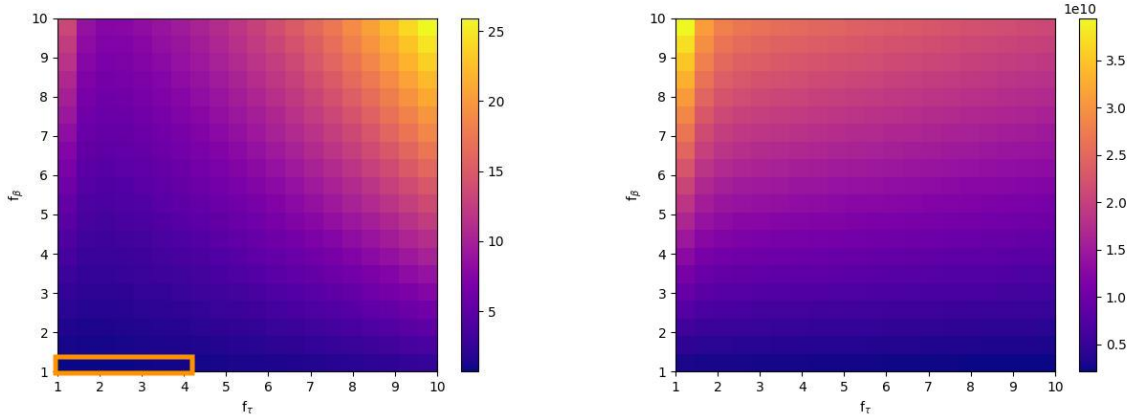

(a) (b)

Figure 14: Competition outcomes for across a portion of the phase space spanned by the LIN-parameters. (a): P/P_r after extinction of host culture. The orange box shows the part of the phase diagram where the ratio is less than 1, meaning the mutant has won. (b): The absolute concentration of WT phages, P, after host extinction.

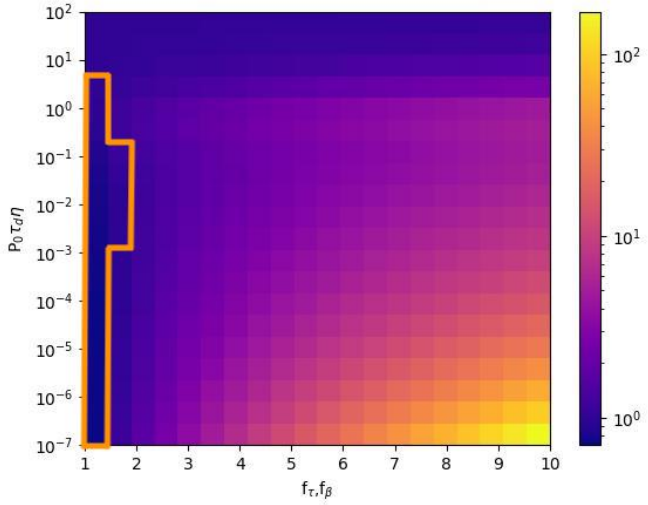

Figure 15: Competition outcome for various combinations of LIN parameters and initial phage concentrations. The plotted values are P/P_r after extinction of host culture. Here, the LIN parameters are kept equal, $f_\tau = f_\beta$. The y-axis is the ratio between the bacterial doubling time $\tau_d = 20$ min and the time $(P_0\eta)^{-1}$ which a cell can on average expect to exist before being infected. For $P_0\tau_d\eta \ll 1$, this quantity represents the probability for a bacterium existing in the initial condition of the simulation to get infected before replicating. The orange box shows the part of the phase diagram where the ratio is less than 1, meaning the mutant has won.

and that plenty of nutrients are still around when the culture succumbs to phage predation ($n(t) \approx n_0$), which is to say that that the growth is entirely stifled by phage infection and not by nutrient depletion. The combination of B_0 and $P_0 = P_{r,0}$ determines how long the culture is allowed to grow, how many cells are infected during growth and the concentrations of infected cells and hosts following collapse of B. For a certain B_0, larger P_0 means earlier collapse of the culture, though the exact relation is non-trivial due to the time-delayed, superexponential growth of P (eq. 16). The culture stops growing once $(P_{tot}\eta)^{-1} < \tau_d \implies P_{tot}\eta\tau_d > 1$, with τ_d the *E. coli* doubling time and $P_{tot} = P + P_r$. To explore a larger part of the space of possibilities spanned by the initial conditions, figure 15 shows a phase diagram varying $f_\tau = f_\beta$ and $P_0 = P_{r,0}$, fixing B_0 to the default value. The LIN advantage here increases with the LIN-parameters, as before, but also decreases with initial concentrations of phages. If P_0 is very small, the bacterial culture is allowed to grow a lot before the phage concentration is large enough to start the collapse of the healthy culture. The greater the peak concentration of the colony, the higher the subsequent concentration of phages, the more superinfections happen, the greater the significance of the sink effect. In figure 15 again, WT almost always wins. For $P_0\eta\tau_d \gg 1$, WT always wins, because the initial concentration of phages alone is enough to make virtually all WT bacteria go into LIN, leading to significant sink effect.

Though this chapter does not by any means cover the space of possible outcomes of this competition simulation, it does make it clear that, in the simulation, the sink effect lends a significant competitive benefit to WT T4 against an r-mutant.

Discussion of broth competition results

It should be noted that in many of the simulations that go into figs. 14a and 15, the LIN'ed bacteria reach MOI's (multiplicities of infection) that are likely higher than what can be achieved in the real world. For high f_τ, the LIN'ed bacteria have a very long time to adsorb *r*-mutants, and in that time they achieve very high MOI's. Figure 16 shows the MOI at different values of f_τ with initial values as in the example

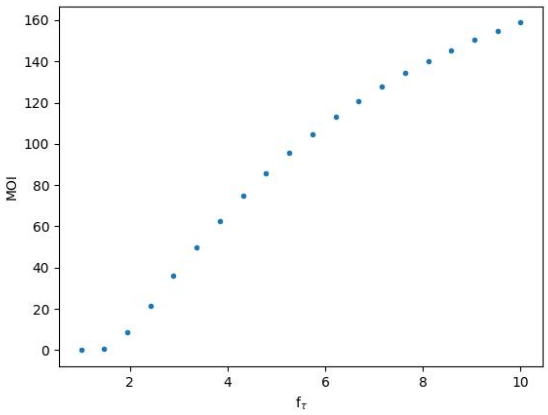

Figure 16: Average MOI of LIN'ed bacteria before they lyse, as function of f_τ. Here $f_\beta = 2$.

simulations. Already at $f_\tau \approx 4$, the MOI starts to exceed 50-70 [9], which is Abedon's estimate of the maximum MOI that a cell can sustain before undergoing lysis-from-without. Obviously, the MOI is not a function solely of f_τ, but also of the initial concentrations. I am not considering lysis-from-without in this project, but it should be taken into account when testing models results in the lab.

The result that WT victory over an *r*-mutant can be largely attributed to the sink effect rests heavily on the mechanism of superinfection exclusion, which applies to T-even phages. If superinfection changed the fate of the cell in any other way, say if a cell produced offspring of both types of two infecting phages, then these results would not apply directly. As I cannot make any statements about the consequences of superinfection in general, there are limits to what I can conclude from these results. Arguably, it is possible that the sink effect only represents a selection *against* rapid lysis mutants, but does not actually benefit a T4 population in competition against an entirely different species of phage.

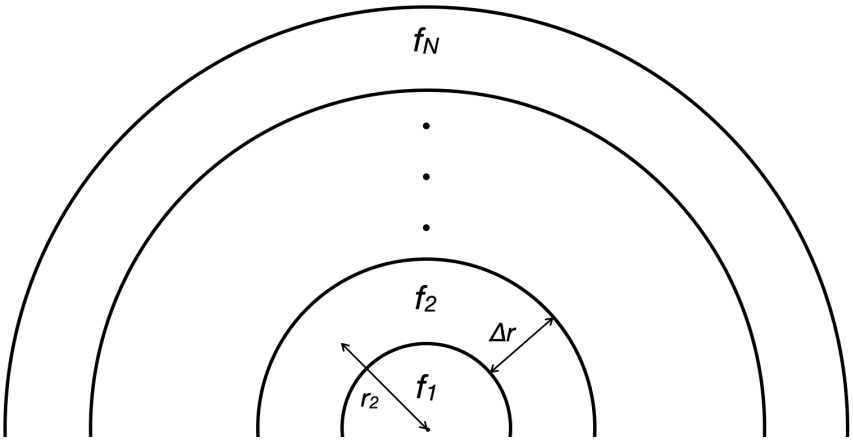

Figure 17: Illustration of the circular grid on which I represent the variables in the plaque models. The distance between cell borders is Δr. The midpoints of the gridcells are at distances $r_i \equiv \Delta r(i - 1/2)$ from the center, and each variable f has a value f_i at each of those distances, representing the concentration in the corresponding gridcell.

5 Modeling plaque formation

Next, I wish to model LIN in a context that allows for spatial variation and propagation. The goal in this chapter is to represent the formation of a single plaque, either WT or r-mutant, from the first infection to the finished plaque as it looks when nutrients are depleted. The plaque models MP0 and MP1 represent all the same reactions as M0 and M1, now taking place in a soft agar which permits diffusion of phages and nutrients while bacteria are fixed in place.

The models are two-dimensional, assuming no relevant dynamics across the thickness of the agar. The variables are represented as area concentrations with the units μm^2. Since plaques expand outward from the point of the initial infection with no preferred direction, I assume radial symmetry, with the initial infection occurring at the center, $r = 0$. The variables now become functions of both space and time ($f(r, t)$), governed by PDE's rather than ODE's. As the variable units change, so must the units on the coefficient in the non-linear infection term ηBP which is replaced by $\eta_s BP$ with

$$\eta_s \equiv \eta/\Delta a. \tag{39}$$

Now, except for the substitutions $\mathrm{d} \to \partial$ and $\eta \to \eta_s$, the differential equations for B, L_i and $L_{I,i}$ are unchanged from the equations in M0 and M1. In contrast, the P and n equations receive a diffusion term. Eq. 10 is replaced with

$$\tfrac{\partial n}{\partial t} = -\tfrac{1}{Y} g_n(n)\, B + D_n \nabla^2 n \tag{40}$$

Eqs. 9 and 24 become, respectively,

$$\tfrac{\partial P}{\partial t} = \beta(n) L_N/\tau(n) + (D_P \nabla^2 - \eta_s\, B_{tot}) P \ \ \text{(MP0)} \tag{41}$$

$$\tfrac{\partial P}{\partial t} = \beta(n) L_N/\tau(n) + f_\beta \beta(n) L_{I,N}/(f_\tau \tau(n)) + (D_P \nabla^2 - \eta_s\, B_{tot}) P \ \ \text{(MP1)} \tag{42}$$

5.1 Integrating the diffusion term

The assumption of radial symmetry allows for efficient computation by using only a single spatial coordinate. It also enables us to integrate the diffusion term with a geometrical method that I take from [31].

Imagine dividing the system (plaque and surrounding lawn) into l equally spaced concentric circles, centered on the plaque, separated by a distance Δr (fig. 17). The spaces between these circles are the gridcells of my radially symmetric lattice. The cells should be narrow enough that we can assume constant concentration of each variable within a gridcell. The diffusion in the system is nothing but the flux of particles through the circles separating the gridcells, which are given the indices $i \in [1, l]$. Since we are interested in the values inside the cells, and not on the borders, the index i will designate a distance $r_i = \Delta r(i - 1/2)$ from the center, ie. equidistant from the two enclosing borders. The neighboring borders are placed at radii $r_{i-1/2} = \Delta r(i-1)$ and $r_{i+1/2} = \Delta r i$. Neglecting other effects than diffusion, the rate of change of the total amount of the variable f in the i'th shell is the difference between the signed fluxes through the enclosing borders.

$$\int_{A_i} \frac{\partial f}{\partial t} dA = \oint_{S_{i-1/2}} \mathbf{J} dS - \oint_{S_{i+1/2}} \mathbf{J} dS = C_{i-1/2} J_{i-1/2} - C_{i+1/2} J_{i+1/2} \tag{43}$$

using the circumferences $C_{i+1/2} \equiv 2\pi r_{i+1/2} = 2\pi i \Delta r$. We see that the boundary condition at $r = 0$ is taken care of already, because the "circumference" $C_{1/2}$ of the innermost "circle" (dot) will be zero. If we assume constant concentration in a shell, we get

$$\int_{A_i} \frac{\partial f}{\partial t} dA \approx A_i \frac{\partial f_i}{\partial t} \tag{44}$$

Combining eqs. 43 and 44 with Fick's law $J = -D\frac{\partial f}{\partial r}$ yields

$$\frac{\partial f_i}{\partial t} = \frac{D}{A_i} \left(C_{i+1/2} \left. \frac{\partial f}{\partial r} \right|_{r_{i+1/2}} - C_{i-1/2} \left. \frac{\partial f}{\partial r} \right|_{r_{i-1/2}} \right) \tag{45}$$

If we use a central discretization scheme around $f_{i+1/2}$

$$\frac{\partial f_{i+1/2}}{\partial r} \approx \frac{f_{i+1} - f_i}{\Delta r}, \tag{46}$$

we get the aproximation:

$$\frac{\partial f_i}{\partial t} \approx \frac{D}{A_i \Delta r} \left(C_{i+\frac{1}{2}} (f_{i+1} - f_i) - C_{i-\frac{1}{2}} (f_i - f_{i-1}) \right) \tag{47}$$

The area of a shell is given by

$$A_i = \pi \left((i\Delta r)^2 - ((i-1)\Delta r)^2 \right) = \pi (2i - 1) \Delta r^2. \tag{48}$$

We can simplify eq. 47 by writing

$$C_{i+1/2}/A_i = \frac{i}{(i-1/2)\Delta r} = \frac{\phi_{U,i}}{\Delta r} \tag{49}$$

$$C_{i-1/2}/A_i = \frac{i-1}{(i-1/2)\Delta r} = \frac{\phi_{L,i}}{\Delta r} \tag{50}$$

$$\frac{C_{i-1/2} + C_{i+1/2}}{A_i} = \frac{2i-1}{(i-1/2)\Delta r} = \frac{2}{\Delta r} \tag{51}$$

with

$$\phi_{L,i} \equiv \frac{i-1}{i-1/2}, \; \phi_{U,i} \equiv \frac{i}{i-1/2} \tag{52}$$

where L is for "lower boundary", U is for "upper boundary". Now,

$$\frac{\partial f_i}{\partial t} \approx \frac{D}{\Delta r^2}\left(\phi_{L,i} f_{i-1} + \phi_{U,i} f_{i+1} - 2f_i\right) \tag{53}$$

For the LHS, I simply use forward Euler. This gives the entire FTCS-type algorithm for the advection term:

$$f_i^{n+1} = f_i^n + \frac{D\Delta t}{\Delta r^2}\left(\phi_{L,i} f_{i-1}^n + \phi_{U,i} f_{i+1}^n - 2f_i^n\right) \tag{54}$$

with n as the index for time coordinates.

For the distant boundary, I use reflecting boundary conditions, $\frac{\partial f(l)}{\partial r} = 0$. In the central scheme, this means $\frac{f_{l+1} - f_{l-1}}{2\Delta r} = 0 \implies f_{l+1} = f_{l-1}$. Of course, f_{l+1}, doesn't exist, but we can use this in the central scheme for the diffusion term,

$$\phi_{L,l} f_{l-1}^n + \phi_{U,l} f_{l+1}^n - 2f_l^n = \left(\phi_{L,l} + \phi_{U,l}\right) f_{l-1}^n - 2f_l^n = 2f_{l-1}^n - 2f_l^n \tag{55}$$

which, for $i = l$, is inserted into eq. 54.

Since I integrate explicitly, the change due to diffusion in a time step is simply added to the change due to reactions (growth, infection, etc). If I gather all the values of f in a vector $\boldsymbol{f}$, the diffusion term can be computed for the entire system with a single matrix product, $\frac{D\Delta t}{\Delta r^2} M\boldsymbol{f}$. The matrix M has

$$M_{i,i} = -2 \tag{56}$$

$$M_{i,j} = \phi_{L,i} \text{ for } i = j+1,\ 1 < i < l \tag{57}$$

$$M_{i,j} = \phi_{U,i} \text{ for } i = j-1,\ i < l \tag{58}$$

$$M_{l,l-1} = 2 \text{ (reflecting BC)} \tag{59}$$

$$M_{i,j} = 0 \text{ else} \tag{60}$$

5.2 Results

The plaque simulations are initialized with a single infected bacterium in the center. Specifically, I set $L_1(t=0) = 1/A_1$ and $L_i(t=0) = 0$ for $i \neq 1$. Soon, phages are produced, they diffuse, infect new cells, and thus reproduce and propagate. Figure 18 shows distributions right after the plaque has stopped spreading. Links to animations are in the caption and the url's are given in appendix A.

The model reproduces some of the qualitative observations from Abedon's plaque experiments, namely that the WT plaque is smaller and that the total concentration of live bacteria, B_{tot}, progresses more gradually from the center and outwards, which in a real plate could conceivably appear as a foggy halo. If we define the width of the plaque as the radius, r, at which $B_{tot}(r) = B_{tot}(r_{edge})/2$, ie. where the the bacterial concentration is half the value at the uninfected lawn, then MP0 gives a radius of 0.50 mm and MP1 gives 0.38 mm. Fig. 18 also agrees with Abedon's conjecture that the halo consists of LIN'ed bacteria.

We can define the ZOI as the area where susceptible bacteria have been significantly decimated by infection. Specifically, I will say that the ZOI is the area with $r < r_{ZOI}$, where r_{ZOI} is the radius which satisfies $B(r_{ZOI}) = B(r_{edge})/2$. Visually, the ZOI then ends where the blue curve begins in fig. 18. If we assume that treatment with chloroform vapor would lyse all infected cells, as Abedon supposes, then the blue curve is what would remain after this treatment. In fig. 18a, the ZOI is 0.62 mm and in fig. 18b it is 0.58 mm. As in Abedon's hypothesis, the ZOI's are more similar in size than the plaque sizes. The ZOI in fig. 18b is 6% smaller than in fig. 18a, while the plaque size is decreased by 24%. Looking further inside the lawn, the tail of the L-curve is all but unchanged by the introduction of LIN.

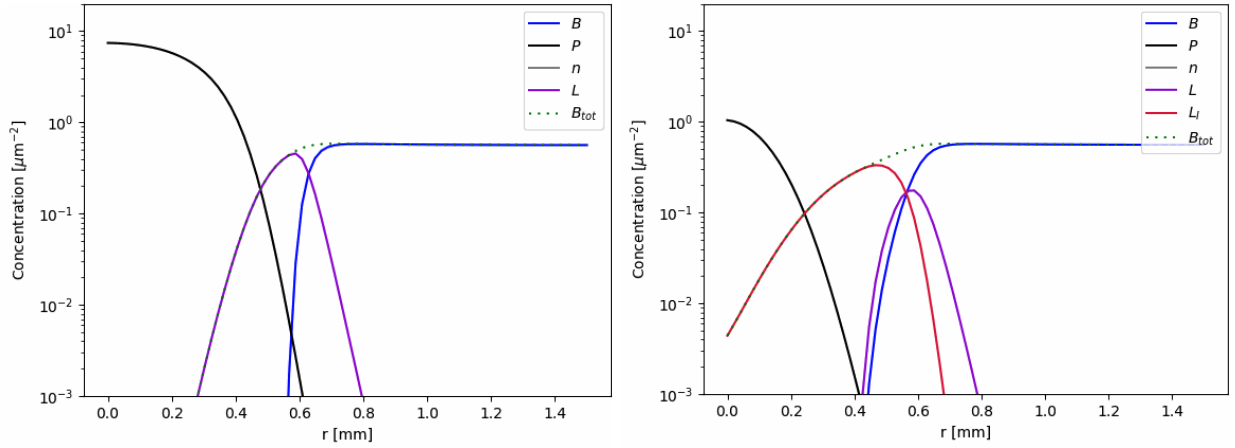

(a) (b)

Figure 18: Plaque simulations after 3 hours. At this point, the nutrients are depleted and the plaque frozen. (a) *r*-mutant plaque. Video. (b) WT plaque with $f_\tau = f_\beta = 2$. Video. The green dotted line shows that the total concentration of live bacteria (which is assumed to correspond to the visible turbidity in the plate) increases monotonically away from the center. The plots show the plaques immediately after they have taken their final shape. If the simulation is continued, the phages diffuse and adsorb to the remaining bacteria until no more free phages are left. Comparing the phage concentrations in this plot is misleading: In terms of free phages, the WT was leading earlier in the simulation, but many have been adsorbed by the LIN'ed bacteria near the center in the time it took the plaque to freeze.

5.3 Plaque expansion

As mentioned in section 2.5, it seems surprising that the WT is able to spread as far in a soft agar as an *r*-mutant when, after some short distance, the cells apparently stop lysing. How do the phages manage to diffuse as far without the aid of continued lysis? According to my models, the infection front consists of a tail of small concentrations of infected cells, extending out into the bacterial lawn at large. At a given time, the phage concentration on the front is low enough that superinfection hardly ever happens, meaning that the front does not "know" whether the phage is able to trigger LIN or not. The following sections will make this clear.

Following a single phage infection on a growing bacterial lawn, the resulting plaque will generally expand linearly in time [32] [27]. The period of linear growth, the "enlargement phase" (Koch, [32]), does not begin immediately, but takes a few rounds of infection and burst to get started. Both MP0 and MP1 reproduce the enlargement phase. To set the stage for further analysis of the difference between MP0 and MP1, I here present a series of different characteristic radii r denoting different positions near the moving plaque edge.

r_{front} represents the front of the expanding infection. Due to the variables being continuous, the front is tricky to define. In a real plaque, there is presumably some distance from the plaque center beyond which exactly zero bacteria have been infected by phages from this plaque. In contrast, in my continuous simulations, L_i have vanishing but non-zero tails spreading out to the edge of the system. As a heuristic, I define r_{front} as the largest r-value where the burst term ($\beta L_N/\tau$) is larger than the diffusion term ($D_P \nabla^2 P$) in the PDE for P (eq. 41). The biological interpretation would be that, above this distance, phages are diffusing outwards, but no infected cells are bursting yet.

$r_{P,det}$ is a rough guess at the radius above which phage concentrations are so low that stochasticity starts to play a significant role. I have set the cutoff at $P = B_0$. The reason for this is that, in soft agar, bacteria exist as microcolonies growing from the initial mother bacterium [27]. The initial bacteria are precisely those that were inoculated on the agar at the outset of the experiment. The concentration of microcolonies,

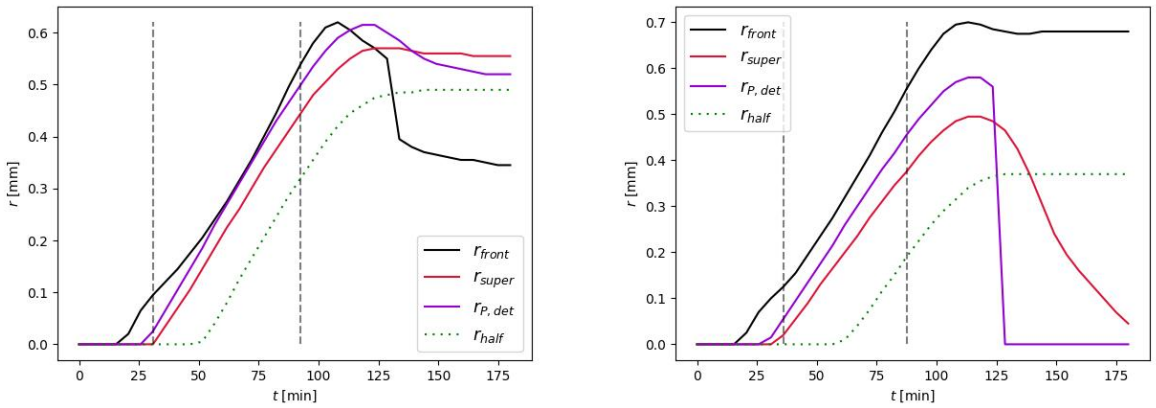

(a) (b)

Figure 19: Visualization of plaque expansion over time. (a) MP0. (b) MP1, $f_\tau = 10, f_\beta = 1$. The vertical dotted lines bookend the enlargement phase, defined as the period in which r_{super} grows with at least 85% of its max speed during a single time-step.

then, remains B_0, even as the concentration of individual bacteria grows. We can expect the assumption of a continuum of phages to break down - and stochasticity to play an important role - in areas where there is less than one phage per microcolony. For this reason, I also track $r_{P,det}$ which is the radius above which $P < B_0$.

Thirdly, I define r_{super} to be the radius at which $P = B$. In the case of high concentrations, such that phages quickly find bacteria and vice versa, two important things start two happen once P reaches B from below. First, bacteria start to get significantly decimated, meaning that the available hosts are about to become scarce. Second, infected bacteria will have a high likelihood of getting superinfected. Thus, in MP0, I can say that $r \approx r_{super}$ is an area where the model *would behave differently* if I were simulating a WT phage. Specifically, a significant fraction of the bursts that happen there would have been inhibited in the WT case.

The last distance is r_{half} which is simply the point at which $B_{tot} = B_{max}/2$, which I take to represent the visible edge of the plaque.

The expansion speed shared by these four different markers is $\approx 8\ \mu$m/min. This agrees quite well with a loose argument one could make based on gaussian distributions emanating from discretized bursts. Since I am modeling simple diffusion, a burst happening at $r = 0$ and $t = 0$ (not necessarily the center and start of the simulation, but simply as reference coordinates) will lead to an expanding gaussian phage-distribution with a volume of $\beta(n) \approx 150$, taking the form

$$\frac{\beta}{4\pi D_P t} e^{-r^2/4D_P t} \tag{61}$$

After τ_l, the phages have on average spread

$$r_{burst}(\tau_l) = 2\sqrt{D_P \tau_l}. \tag{62}$$

ie. the standard deviation $\sigma(\tau_l)$. Neglecting the time it takes to find a new host, the next set of bursts happens after $t = \tau_l$, and the average position of these bursts will be $\sigma(\tau_l)$. On the far side of this second

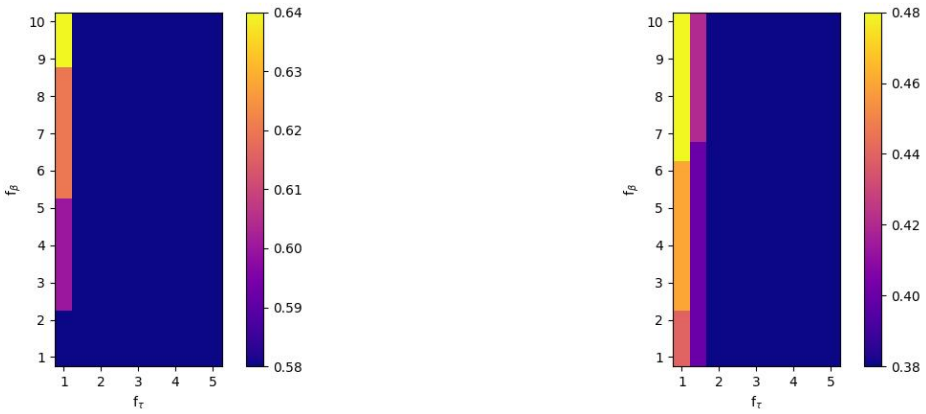

(a) (b)

Figure 20: Phase diagrams for MP1. (a) Zone if infection (ZOI) radius. (b) Plaque radius. The pixellated appearance is due to the spatial resoltion $\Delta r = 20\mu$m.

burst, we can neglect the gaussian from the original burst at $r = 0$, since the speed of that burst decreases monotonically and will forever be expanding more slowly than subsequent bursts. The average speed with which the bursts propagate out from the initial burst then becomes

$$v = 2\sqrt{\frac{D_P}{\tau_l}} \approx 7\ \mu\text{m/min} \tag{63}$$

I have confirmed that this dependence on D_P and τ_l holds within a factor 4 of those parameters.

All of the plaque markers give approximately the same expansion speed, though they do not place the beginning and end of the enlargement phase at the same time. The parallel ascending lines in fig. 19 tell us that the overall form and content of the plaque edge does not change during enlargement, even though absolute particle concentrations grow with the bacterial lawn. The WT plaque expands with the same speed as the mutant plaque, but r_{half} is delayed, leading to a smaller plaque. Note that r_{front} actually reaches a higher value in MP1 than in MP0. This is presumably due to the fact that, since less lysis is inhibited within the plaque, less phages diffuse out to the edge, meaning that you have to go to higher r-values to find the place where diffusion wins over burst. I do not take it to mean that infection has spread farther in MP1 which, based on fig. 18, is evidently not true. The shift in r_{front} speaks to the fact that the definition of r_{front} is not particularly solid.

In both models, the maximum value of $r_{P,det}$ is very nearly equal to the ZOI. Note also that in both models, but particularly MP1, $r_{front} > r_{P,det}$. This might correspond to the observation in fig. 6 that, following chloroform treatment, both types of plaques display a slightly darkened area outside a sharp edge. This is most clear in the case of the r-mutant, but close inspection shows this to also be true for the WT-plaque, whose sharp-edges zone has a slightly smaller radius than that of the r-mutant.

How to extend the wild-type zone-of infection beyond the visible plaque

As with the broth models, let us look at the results across a wider parameter space, again varying f_τ and f_β. Fig. 20 shows that the plaque size and ZOI are virtually insensitive to these parameters. The variation mainly happens at the left edge with $f_\beta \gg f_\tau$, which is not biologically meaningful. The large blue swaths that fill the rest of the phase diagrams are due to the fact that, above a certain value of f_τ, LIN'ed cells never

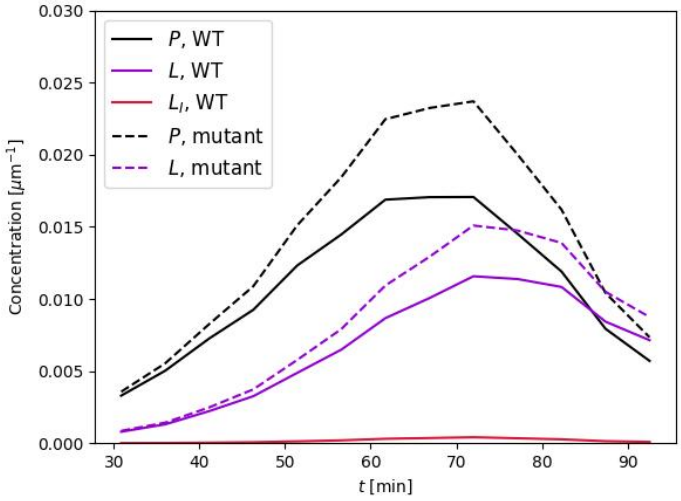

Figure 21: Concentrations at r_{front} for both MP0 and MP1 with $f_\tau = 10, f_\beta = 1$. The distance r_{front} is determined only in MP0, so that the same time and space coordinates are used in selecting values from both MP0 and MP1.

lyse, and so the exact values of the LIN parameters become inconsequential.

Fig. 20a tells us that the fact that the ZOI is nearly unchanged by the introdution of LIN (recall it was 0.62 mm for MP0) does not depend on a specific choice of LIN parameters. How does the WT manage to spread as far despite keeping many cells alive? Recall that all the markers on the plaque edge that I have defined move at the same velocity, and that this velocity is purely a function of D_P and τ_l. The plaque expansion does not accelerate as concentrations increase, and it does not decelerate until nutrients become significantly depleted. Imagine that, at some point during the enlargement phase, I set P and L to zero for $r < r_{front}$. The front remains intact but is subsequently deprived of the diffusive supply of phages that was coming from within the plaque. This is, in a sense, a cartoon version of LIN, since LIN precisely inhibits lysis some distance within the plaque, and thus robs the front of the phages that would otherwise diffuse out from those bursts. However, r_{front} is now effectively a new inoculation point (or a series of inoulation points spread out on a circle) and it will expand linearly outward with the same speed as it did before, according to the same logic of sequential expanding gaussians.

Fig. 21 shows $P(t, r = r_{front})$ and $L(t, r = r_{front})$ for both MP0 and MP1. Note here that for all curves, r_{front} is defined from the MP0 simulation. It is not redefined in MP1, which would place it at slightly different positions. Here, $f_\tau = 10$ and $f_\beta = 1$. The large f_τ means that LIN'ed cells never lyse. We see that the front does feel the LIN happening within the plaque, as this results in lower values of both P and L. However, the values do not vanish, and they follow the same temporal form. It seems that LIN does not affect the ability of the front to sustain its own continued propagation during the enlargement phase. The figure also shows that the number of superinfected cells at the front is always negligible, which is a natural result of the low P-concentrations here.

5.4 Discussion of plaque morphology

There is a significant discrepancy between fig. 18 and Abedon's experiments. Upon treatment with chloroform, the sharp edge of the r-mutant plaque does not budge. If I remove the L-curve in fig. 18a, this increases the plaque radius from 0.50 mm to 0.62 mm. To reproduce the unchanged plaque size, I must have all the infected cells lyse in fig. 18a, while not having all the LIN'ed cells lyse in fig. 18b. The reason

that some infected cells remain is that I have set $r_l = 0$, so that infected cells stop transitioning when nutrients are depleted. Given the way I am modeling $\tau_l(n)$, I am forced to do this, otherwise the plaque will grow indefinitely, and the simulation will be useless.

The solution could lie in a different way of modeling $\tau_l(n)$. Incidentally, Rabinovitch et.al. have shown that, in some conditions, the lysis time actually has a peak at a certain value of the culture doubling time, and that above that peak, slower growing hosts lyse *faster* [20]. As bacterial growth slows down, burst size also approaches zero, so that the fast-lysing cells produce very few virions. Implementing this model in MP0 would mean that, once the nutrients start to run out, the remaining infected cells would immediately lyse, releasing very few new phages and only healthy bacteria would be left, meaning that chloroform treatment would not affect the plaque size, in agreement with fig. 6. It should be noted, though, that the model in [20] is fitted to experiments where the growth conditions are varied by changing the *type* of nutrients, not due to nutrient depletion. It is not guaranteed that the model would apply one-to-one to nutrient depletion.

Incorporating this alternative model of $\tau_l(n)$ in MP0 and MP1, in order to get the L curve to vanish with the nutrients, would force me to give up the assumption that $\tau_{l,I}$ and τ_l depend on n in the same way, in order to preserve the L_I curve and thus still reproduce the WT halo. As explained in chapter 2.3, the experimental literature does not, as far as I can tell, lend itself to a simple quantitative relationship between host growth rate and LIN'ed lysis time, such as the one proposed in [20] for non-LIN'ed lysis time. The decision to apply the same model to both types of infected and just set $\tau_{l,I} \propto \tau_l$ is purely for simplicity and not based on experimental results. The molecular model of LIN, in fact, gives us a good reason to assume that the lysis-time of a WT and an r-mutant should *not* have the same n-dependence, since the molecular clocks are totally different: In the former case, lysis relies on the degradation of RI, while in the latter case it is triggered by a sufficient buildup of holin in the plasma membrane. In conclusion, assuming Abedon's interpretation of the effect of chloroform treatment is correct, the discrepancy between MP0 and real mutant plaques is an indication that, in order to reproduce the difference between WT and r-mutant plaques both before and after chloroform treatment, one should treat $\tau_{l,I}$ differently from τ_l, in regards to their dependence on n.

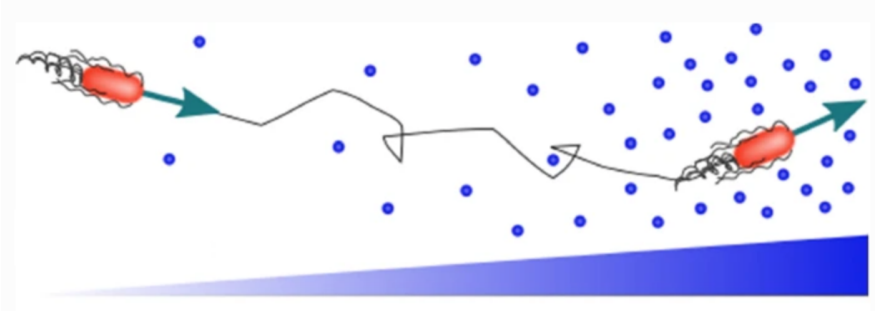

Figure 22: Illutration of the mechanism of chemotaxis. Blue: Chemoattractants (nutrients). The kinks in the trajectory represent places where the cell stopped to "tumble" and change direction. After a tumble, the new direction is random, but the cell will modify the duration before the next tumble depending on the change in nutrient concentration it experiences during a run. The resulting overall movement is biased towards higher nutrient concentrations. From Jakuszeit et. al. ([35]).

6 T4 and swimming bacteria

If the environment allows, *E. coli* moves through its surroundings using the well-known "run-and-tumble" mechanism called chemotaxis [33] [34], illustrated in fig. 22. Aided by its flagella, the cell swims in a straight line until, at a random time, it stops, "tumbles" in place, and then starts swimming in a new, random direction. If during a run the cell enters an area of increased nutrient concentration, it senses this with chemoreceptors on its surface, leading it to decrease its rate of tumbling and, as a result, move farther into this area. If it senses the nutrient concentration decrease, it it will tend to tumble sooner. The emergent result is that a cell, on average, will move along gradients of nutrient concentration.

Connecting this to T4 infection dynamics, imagine an infecting phage whose host has just been superinfected, and imagine that this host is able to swim in its current environment. The superinfection signals high density of phages, which in turn signals that, until recently, there was a high density of nutrient-eating bacteria. Since it is drifting up along nutrient gradients, the superinfected cell may soon find itself in a nearby area that is richer in nutrients, and this richness may be an indication that the new area is still relatively unpopulated by bacteria, and thus phages. If this scenario is in fact a common occurrence for a T4-superinfected cell in nature, this would present a clear incentive for the phage to postpone lysis in response to superinfection. If it lets the host travel to this new area before lysing, its progeny will be released in an area which is not only less dense with phages but is also a magnet for new hosts, and those hosts may even multiply there due to the large amount of available nutrients.

Since the incentive is so clear in the story presented above, an examination of the reproductive advantage of LIN should also take chemotaxis into account. In the following sections, I present the models MS0 and MS1, and the results I have produced so far. In the process of developing and analyzing these models, I have encountered many computational challenges, and I will describe these. I also present some of the qualitative predictions of the simulated experiment. Because of said challenges, I have not managed to make many conclusions about what the models tell us about the ecological effect of LIN. This question warrants further analysis of the models or altered versions of them.

The experimental setup

A chemotaxis experiment can be performed in a setup similar to that of plaque experiments but using a medium which has a lower concentration of agar - about 0.3% works [25]. Such a medium will allow individual bacteria to propagate slowly through the medium, while still preserving spatial heterogeneity, as opposed to liquid cultures. If bacteria and phages are inoculated together in a point, we can assume

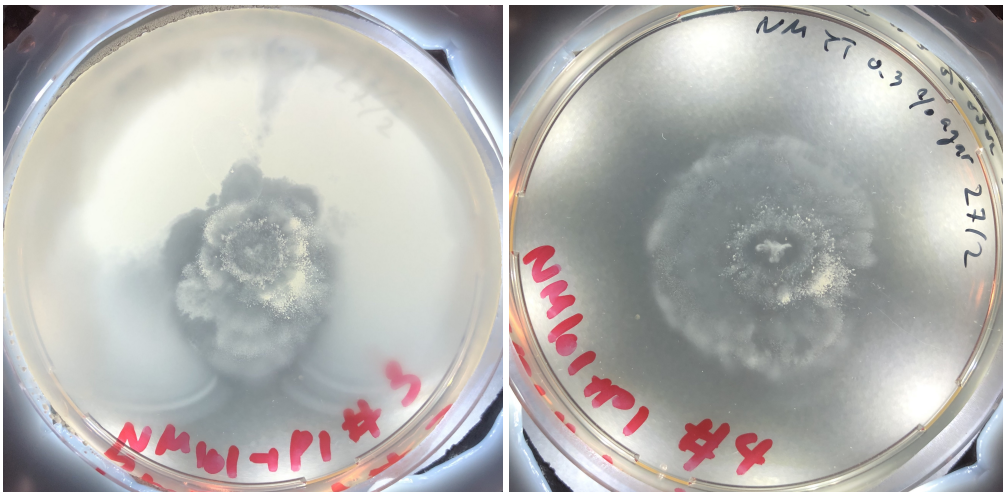

(a) (b)

Figure 23: Swimming plates made by Namiko Mitarai, containing phage T4 and *E. coli*. Plate diameter is 9 cm. (a) WT. (b) r-mutant.

radial symmetry of the system around that point and use the same circular grid as in the plaque models (fig. 17).

An example of the type of swimming experiment I simulate is shown in fig. 23. Here, a drop containing both phages and bacteria is inoculated into the agar in the middle of the plate. As bacteria consume nutrients around the inoculation spot, they are driven by the mechanism of chemotaxis to spread farther out into the medium. As is evident, this type of experiment can yield results of much higher complexity than plaques. In particular, the WT case in fig. 23a is far from radially symmetric around the inoculation spot, and it displays many different visual textures. This attests to the difficulty of designing a replicable swimming experiment. The asymmetry can be caused by inhomogeneities in the agar, disruption of the agar upon inoculation, or bacteria developing T4-resistance, to name a few things. Decent symmetry has been achieved in past swimming experiments using different phage species [25], [36]. I do not know of any previous experiments with phage T4 in swimming medium. The results in fig. 23 are preliminary, and Namiko Mitarai is currently working on developing an experimental protocol that yields symmetric and replicable results.

It would be very interesting to see how this plate would react to chloroform treatment, as this might tell us that we can see from the textures of the culture which areas (if any) contain LIN'ed cells.

6.1 Chemotaxis as diffusion plus advection

One way of modeling the stochastic run and tumble of chemotaxis in a well-mixed model is to combine diffusion and advection. This method is used in [25], where chemotaxis is represented by the terms

$$\frac{\partial f}{\partial t} = ... + D_B \nabla^2 f - \nabla \cdot (f \cdot \vec{v}(n)) \tag{64}$$

where $v(n)$ is the swimming speed given the current nutrient distribution. In terms of the equations, the swimming models, MS0 and MS1 are identical to MP0 and MP1 expect that the PDE's for B, L_i and $L_{I,i}$ receive the terms in eq. 64. Then, apart from eqs. 40 41 and 42, the MS models consist of

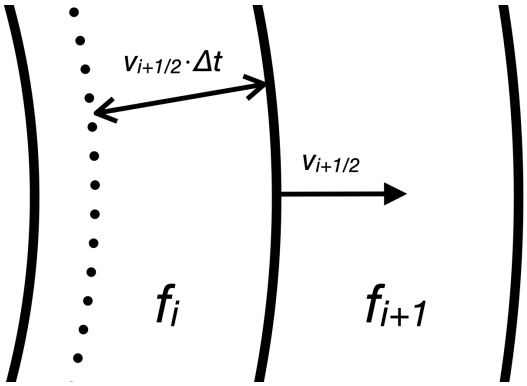

Figure 24: Illustration of the advection algorithm. Here, $v_{i+1/2} > 0$. ΔA_i refers to the area enclosed by the dotted circle and the solid circle to the right of it. That area has constant concentration f_i. All particles of type f in that area are moved from cell i to $i+1$ in a time step.

$$\frac{\partial B}{\partial t} = g_n B - \eta_s BP + D_B \nabla^2 B - \nabla \cdot (B \cdot \vec{v}(n)) \tag{65}$$

$$\frac{\partial L_i}{\partial t} = ... + D_B \nabla^2 f - \nabla \cdot (L_i \cdot \vec{v}(n)) \,,\; i \in [1, N] \tag{66}$$

$$\frac{\partial L_{I,i}}{\partial t} = ... + D_B \nabla^2 f - \nabla \cdot (L_{I,i} \cdot \vec{v}(n)) \,,\; i \in [1, N] \;\; \text{(MS1)} \tag{67}$$

where "..." represents all the appropriate infection, superinfection, transition and lysis terms known from eqs. 18-23.

In some media, the molecules that are sensed (chemoattractants) are not the same as the molecules that are metabolized (nutrients). I have not included this nuance in my models, but it is taken into account in [25]. Taking the functional form of the advection speed from that paper, but letting it depend on nutrients instead of chemoattractants, I get the speed:

$$v(n) = \chi \cdot \nabla \log\left(\frac{1 + n/a_-}{1 + n/a_+}\right) = \chi \cdot \frac{\partial}{\partial r} \log\left(\frac{1 + n/a_-}{1 + n/a_+}\right) \tag{68}$$

where the last equality uses the assumption of radial symmetry. As we discretize space, the variables become vectors: $n \to n_i$ (pardon my recycling the i from states L_i). If we define a vector $a_i = \log\left(\frac{1+n_i/a_-}{1+n_i/a_+}\right)$, the central scheme for v becomes

$$v_i(\mathbf{n}) \approx \chi \cdot \frac{1}{2\Delta r} \left(a_{i+1} - a_{i-1}\right) \tag{69}$$

At the inner boundary $r = 0$, I use the forward scheme instead, and at the outer boundary $r = R_{max} = l \cdot \Delta r$, I fix $v = 0$. The latter boundary condition will not have any effect in practice, because I only use simulation results where no particles have reached the boundary.

6.2 Integrating the advection term

As with diffusion, I forget about the differential form and derive an advection scheme geometrically. The general idea is this: Iterate over each gridcell, starting at $i = 1$ and calculate, based on the speed $v_{i+1/2}$ at the upper boundary of the gridcell, the amount ΔF_i of variable f it exchanges with gridcell $i+1$. $\Delta F_i > 0$

means flow from cell i to cell $i+1$ (outward), while $\Delta F_i < 0$ means flow from cell $i+1$ to cell i (inward). $v_{i+1/2}$ is approximated using linear interpolation of v_i (eq. 69).

The idea is illustrated in fig. 24. Assuming a constant $v_{i+1/2}$ in the vicinity of the border, each particle in the area ΔA_i of the shell separating two concentric circles with radii $r = i\Delta r - v_{i+1/2}\Delta t$ and $r = i \cdot \Delta r$ (ie. the gridcell border) travels from cell i to cell $i+1$.

$$\Delta A_i = \pi \left((i\Delta r)^2 - (i\Delta r - v_{i+1/2}\Delta t)^2 \right) = \pi v_{i+1/2}\Delta t \left(2i\Delta r - v_{i+1/2}\Delta t \right) \tag{70}$$

Notice here, that a negative speed will translate into "negative area", which, in the following, will translate into negative (inward) flux. To find the amount ΔF_i to be transported we need to evaluate the sign of $v_{i+1/2}$:

$$\Delta F_i = f_i \cdot \Delta A_i \text{ if } v_{i+1/2} > 0 \tag{71}$$

$$\Delta F_i = f_{i+1} \cdot \Delta A_i \text{ if } v_{i+1/2} < 0 \tag{72}$$

since the flux comes from either the left or the right side of the border. Now we can calculate the value of f in the next time step:

$$f_i \to f_i - \Delta F_i / A_i \tag{73}$$

$$f_{i+1} \to f_{i+1} + \Delta F_i / A_{i+1} \tag{74}$$

As mentioned, $v < 0 \implies \Delta A < 0 \implies \Delta F < 0$, which gives flux in the inward direction, as required. Note that the algorithm only makes sense if

$$\left| v_{i+1/2} \right| < \Delta r / \Delta t. \tag{75}$$

You may ask: Why not interpolate the variable f as well and calculate ΔF_i from $f_{i+1/2}$? If we can replace $<$ with $\ll$ in eq. 75 (which will be the case in practice because the diffusion algorithm requires that I take Δt down with the *square* of Δr while a quite small Δr is required for convergence of the result as we will see) only particles very close to the border will be transported in a time step, meaning interpolation at the border might be more precise. Also, the evaluation of the sign of the speed would then be unneccessary. The reason is, if I interpolate f_i, I am transporting "fictional" quantities, and this opens the door to problems like negative concentrations. I find the algorithm is more transparent if I do not interpolate, but it is possible that this could solve the convergence problems I discuss later.

6.3 Error analysis on swimming models

Modeling chemotaxis is a lot more tricky than modeling diffusion. For that reason, my simulation results come with some caveats regarding accuracy. The necessity of high spatial and temporal resolution, and the long resulting computation times, make the model more cumbersome to work with and I have in fact not been able to achieve an acceptable convergence of results with increasing spatial resolution, though it does appear to be possible. The necessity of very high resolutions has also made it infeasible to perform parameter scans like I have done with the previous models. In addition, the simulation outcomes are much more messy and varied than in the previous models, making it harder to define global quantitative measures analogous to eg. plaque size.

The simulations turn out to give qualitatively very different results depending on the nutrient richness, ρ, presented in chapter 3. Recall the distinction drawn in chapter 3 between ρ (units ml^{-1}) and $n_0 = \rho\Delta a$ (units μm^2). It turns out that the swimming simulation will display one of three possible "modes"

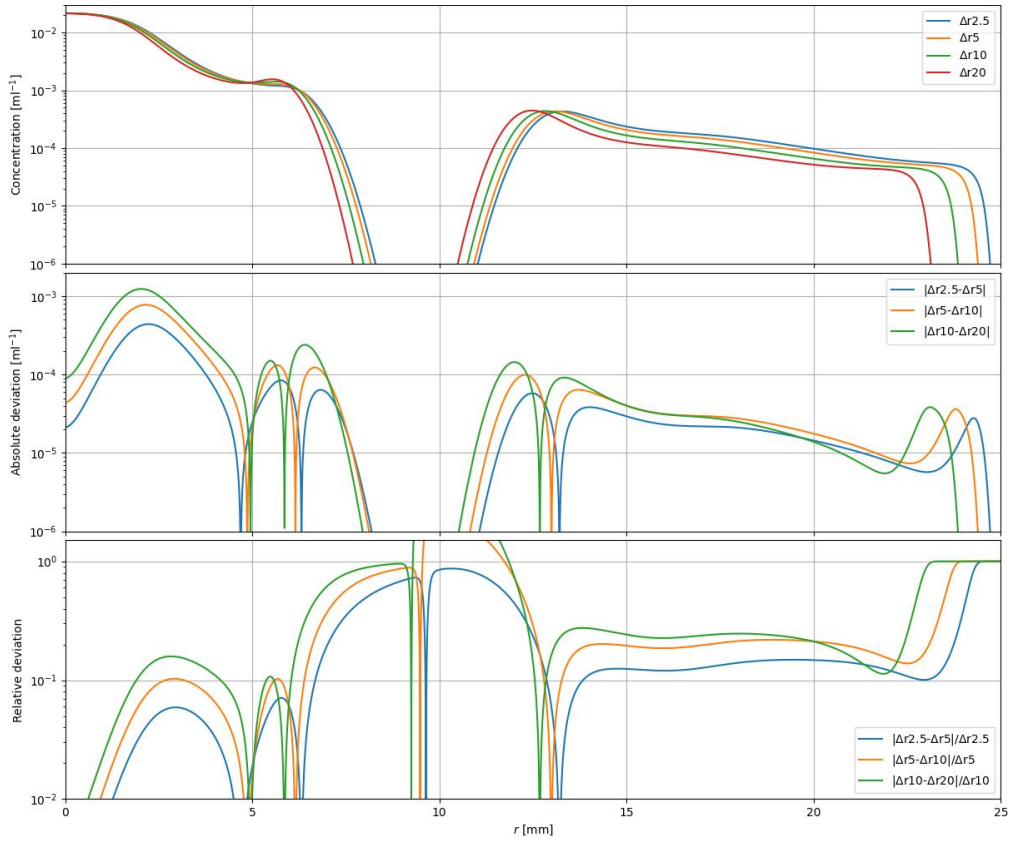

Figure 25: Result on MS0 (r-mutant) simulation for varying spatial resolutions, as well as deviations between different runs. $\rho = 2.5 \cdot 10^6$ ml^{-1}. The simulation has run for 10 hours. The plotted variable is B_{tot}, total number of live bacteria, but the curves are labeled with the spatial resolution. The resolutions Δr are separated from eath other by a factor of 2, and the temporal resolution is fixed to $\Delta t = \Delta r^2/D_n/3$. Top panel: $B_{tot}(r, t = 10\text{h})$ for different spatial resolutions. Middle panel: Absolute deviation between the result of value Δr and that of $2\Delta r$. Bottom panel: Relative deviation. Note that wherever the curves in the top panel cross each other, this is seen as very extreme slopes in the deviation plots. This is because the deviation shifts from a non-vanishing value of one sign to a non-vanishing value of the opposite sign over a short distance, and the log plot makes this shift appear dramatic.

depending on ρ, but independently of Δa and thus the total amount of nutrition in a column of the medium.

Before addressing these modes further, I will start by noting that the mode which emerges at intermediate ρ-values, $\rho \sim 3 \cdot 10^6$ ml^{-1} displays quite complex behavior, featuring large oscillations near the bacterial front and resulting spatial waves behind that front. The reason why I address this mode first is that here, the simulation result converges very slowly with increased spatial resolution, and computation time becomes prohibitive before a satisfactory convergence is achieved. It does, however, appear to converge. Before analyzing simulation results, I would like to address the problem of convergence.

Fig. 25 shows the effect of increasing the spatial resolution on the distribution of B_{tot} in an example run of MS0. The lowest resolution has $\Delta r = 20\mu$m and the resolutions differ by factors of 2, with the smallest gridsize being $\Delta r = 2.5\mu$m. In the top panel we see the actual simulation results, in terms of total bacteria, and it is apparent that, though the curves are not identical, they do have the same overall shape.

The middle panel shows absolute concentration differences between each pair of Δr and $2\Delta r$. As one would hope, the difference between the smallest pair $\Delta r = 2.5$ and $\Delta r = 5$ is smaller than the others - but not by a lot. This is what we mean when we say the result converges slowly. It complicates things significantly because the diffusion algorithm sets an upper bound on the value of Δt which is proportional to Δr^2, meaning that computation time scales as spatial resolution to a power between 2 and 3 (less than

3 because vectorized computation means that the computation time per iteration grows less than linearly with number of gridpoints). The requirement for the FTCS diffusion algorithm on a rectilinear grid is $\Delta t < \Delta x^2/D$ [37] and, through trial and error, I have found that my particular model is stable for $\Delta t < \Delta r^2/D_n/3$ and that, for the resolutions I am working with, this is sufficient not just for stability but also for convergence in the *temporal* resolution.

Generally, the absolute deviation is small in areas where the absolute numbers are small (eg. $r \approx 10$ mm), as we would hope. However, the bottom panel shows, that the absolute deviation does not follow the absolute value linearly. That is to say, there is a tendency for the relative deviation to be quite large, even exceeding 100%, in areas of vanishing absolute concentration. In and of itself, relative deviations of 100% should lead one to discard the result as useless. However, on afterthought, these deviations might be the least significant, in terms of the credibility of the simulation result. If the true solution to the model is anything like the results in the top panel of fig. 25, then it has areas where the concentration will change by many orders of magnitude over a distance of one or two mm (eg. in the interval $r \approx 6$ mm to $r \approx 7$ mm). In that case, since the particles in the simulation propagate through space, it is natural to expect that a tiny relative error in an area of high concentration will soon lead to an enormous relative error in a nearby area of, by comparison, vanishing concentration. Conversely, a large relative difference in the area of low concentration will have a vanishing effect on the outcome in areas of high concentration, since the particles making up this error will get diluted. For this reason, I think both the relative and absolute deviations should be taken into account in a nuanced discussion of the usefulness of the results. Having said all this, I believe the biggest stain on the result is the fact that I have not been able to achieve convergence better than 10% in the area between ≈ 13 and ≈ 22 mm.

The steep slopes close to the right edges of the deviation plots are due to the different resolutions resulting in slightly different swimming speeds, meaning that the errors are large close to the bacterial front which has a steep slope. Note, in that context, that in the top panel the fronts lie closer to each other for smaller Δr, which would seem to indicate that the effective swim speed is converging with decreasing Δr. Note too, that there are r-values where the blue curve in the bottom panel actually lies *above* the other curves (eg. $r \approx 13$ mm), which would seem to refute my assertion that the algorithm is convergent. This generally happens in areas of high curvature in the relative error-plots. The convergence is slow not just in the vertical, but also in the horizontal direction, by which I mean that the as the resolution is changed, the propagation speed increases (hopefully and presumably asymptotically) and so the whole system is stretched in the horizontal direction, leading to points of intersection between the relative error-curves.

The silver lining to all of this is the fact that, in the bottom panel, the relative error does actually decrease with Δr. This is promising, since it makes it reasonable to assume that the algorithm actually does converge. However, we can also conclude that simulation results using $\Delta r \geq 2.5$ - which is what I will be using due to computational limitations - should be taken with a grain of salt. At the same time, as the general conclusions I make on the swimming algorithm are robust to various changes of parameters and initial conditions, I find that they are worth including despite the caveats I have presented. The above analysis does not give us any reason to assume that going to the convergence resolution (assuming it exists) would force me to alter my conclusions on the model.

A final comment on the error: Due to time constraints, I have performed the error analysis on limited simulations, by which I mean a smaller system ($r_{max} = 40$ mm instead of 75 mm) over shorter time (10 h instead of 50 h). It would have been more rigorous to perform the error analysis on an identical system to the one from which I will be making my conclusions. Given more time, this is what I would have done. I have run a few $\Delta r = 2\mu$m simulations corresponding to the ones I include in my analysis and concluded that, though they differ visibly, they do not differ in ways that could alter any of my conclusions. The 2 μm simulations took ~ 20 days to run.

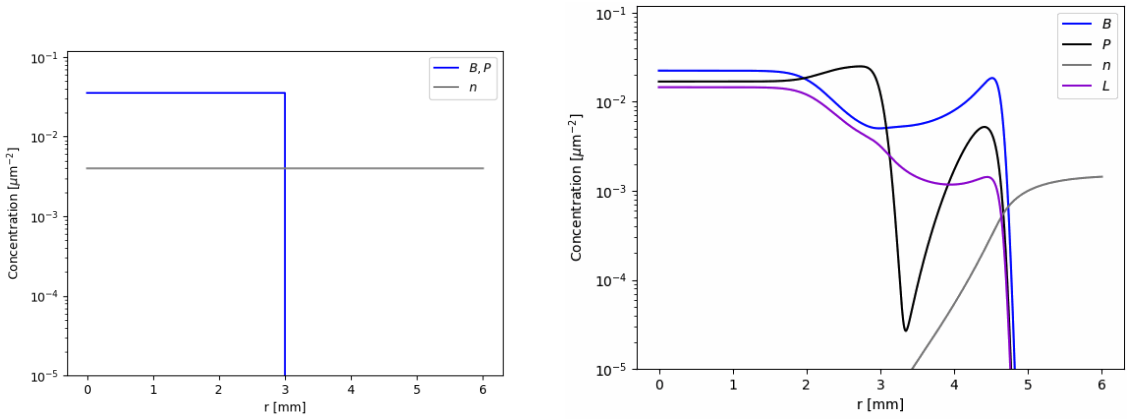

(a) (b)

Figure 26: The initial transient behavior of MS0. (a) The initial condition. (b) The system after 20 min. Though the simulations results display various modes depending on ρ, they share some patterns in the first doubling/latent period. Video.

6.4 Results

As with the plaque models, links to animations are included in captions and in appendix A. The system starts with step-function distributions of B and P (fig. 26a), representing a drop inoculation containing both bacteria and phages. In the first moments of the simulation, it undergoes some transient behavior before settling in to one of the three modes mentioned in chapter 6.3, where the front either oscillates or moves at constant speed. The richness, ρ, of the medium determines the mode of the ordered post-transient behavior. This is true for both the WT simulation MS1 and the mutant simulation MS0. In fact, for smaller values of f_τ, the qualitative outcome is to a large degree conserved upon introduction of LIN. All three modes share somewhat similar behavior during the transient period, and I will start by presenting this before looking at the types of stationary states that are accessible after the transient.

The transient period

Figure 26 shows the initial condition for MS0 and the result after 20 min, ie. a single doubling/latent period. Here, $\rho = 3 \cdot 10^6$ ml^{-1}, but the following qualitative statements about fig. 26 could also apply to the transient for other values of ρ, though they will of course differ in quantitative terms. The reason why the first doubling period shows similar behavior independently of ρ is that the initial condition is the same, meaning that the first generation of susceptible bacteria, as well as the phage population which preys on it, is always the same. The second generation will differ depending on the growth conditions of those bacteria from the first generation that did not get infected.

Looking at fig. 26, after 20 min, the bacterial front has moved ≈ 2 mm and B has formed a peak near the front, resulting both from the advection of bacteria behind the front and from the higher growth rate at the front where nutrients have been depleted to a lesser degree. P shows a deep trough at a radius slightly larger than the inoculation radius as well as a peak on either side of the trough. These peaks represent the offspring of infected bacteria of the first generation. The peak on the right consists of phages that were lysing on the swimming front, while the phages in the peak on the left were released by cells that did not make it on the front and are stuck, since no nutrient gradient remains to guide them away.

Notice that, since nutrients have been totally depleted behind the front, neither advection nor lysis can happen there, and except for diffusion which tends to smooth out curves over time, everything behind the front is more or less frozen. This means that for $r < r_{front}$, the values there roughly tell the story of what

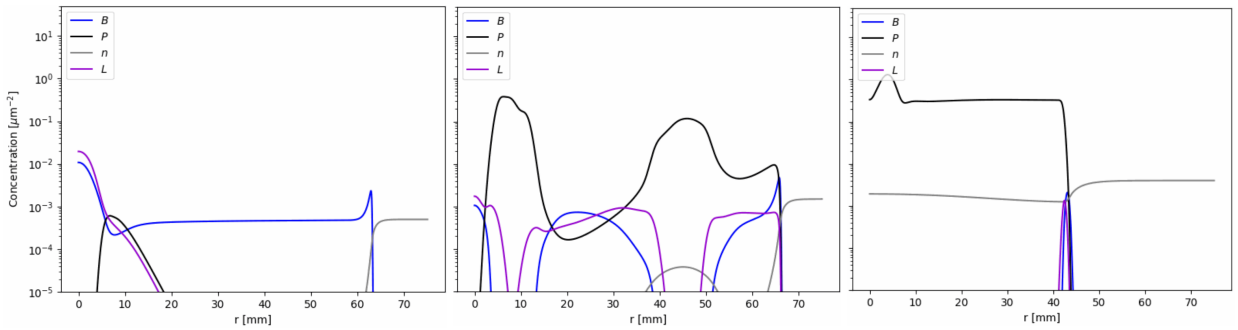

(a) (b) (c)

Figure 27: Three different modes of behavior in a swimming plate. (a) $\rho = 10^6$ ml^{-1} at $t = 20$ h. Video. (b) $\rho = 3 \cdot 10^6$ ml^{-1} at $t = 30$ h. Video. (c) $\rho = 8 \cdot 10^6$ ml^{-1} at $t = 50$ h. Video. In all these simulations $\Delta r = 5$. Note from the t values that the average swimming speed gets progressively slower from (a) to (c). Between (a) and (c) this is due to the much steeper nutrient gradient in (a). In (b), the nutrient gradient at the bacterial front changes over time, and so the propagation speed changes over time.

the front was doing when it passed that point. At any given time, the only place that contains both nutrients and bacteria is the front, and thus all interesting dynamics are happening there. For this reason, it may be helpful in following the animations, to think of the front as a zero-dimensional system. which is, as it were, being fed nutrients "from the right" while expelling cells and phages "to the left". Interestingly, it is possible to achieve analogous modes in the chemostat-version of the zero-dimensional models, which precisely provides a continuous influx of nutrients while expelling material to preserve aproximately constant volume. Appendix C shows the chemostat version and presents results in the oscillatory mode.

After the transient

After the first lytic cycle, the system is ready to fall into the mode that is determined by ρ. The number of phages that have just been released in fig. 26b is approximately independent of ρ, since they were created in the fixed first generation of cells. What happens next, however, is determined by the density of the culture that these phages are released into. If nutrients are scarce, the culture will be relatively dilute, and the chance for a phage of finding a cell before the front has moved on is small. If it is sufficiently small, the basic reproductive number of a phage will be less than 1, and P will decay on the front, which is what we see in fig. 27a, where the decay looks exponential.

If the medium is rich enough, it will be so dense with host bacteria that phages can grow rapidly at the front, until they are abundant enough to decimate the culture locally. Because of the delay in lysis, the phage peak is always a few mm behind the very edge of the front. While it is possible for phages to diffuse to the very edge of the front if the P-peak is high enough, lysis only ever happens some distance behind the front, because of the time delay in lysis. This means that, while the culture can get wiped out right behind the front, there are always enough survivors at the edge for the front to keep moving, allowing the cycle to repeat. The result is the wavy pattern in fig. 27b. That snapshot is taken at a time point where bacteria are abundant at the front but will soon be wiped out by the growing phage population there. I call this mode the oscillatory mode.

As ρ is increased, the oscillations become gradually less violent, and around $\rho = 8 \cdot 10^6$ ml^{-1} they have died out completely. Above this value lies the third mode, shown in fig. 27c. It now takes more bacteria to consume the larger amount of nutrients, but the bacteria are not permitted to grow very much, because the density at which they can be stifled by phages has not increased. Fig. 28a shows this situation in more detail. The system has found a balance between the temporal and spatial dynamics. At the bacterial front,

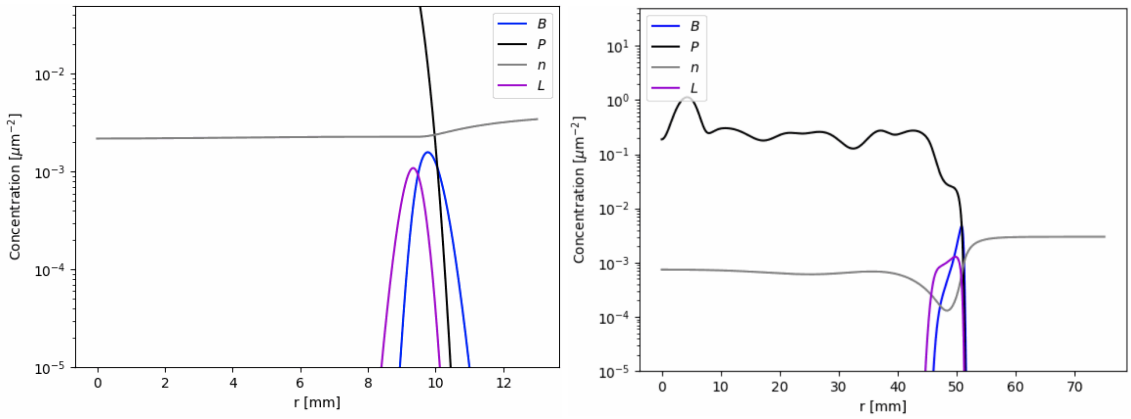

(a) (b)

Figure 28: (a) Crop-in on the front in the third mode, ie. fig. 27c. (b) An example of an intermediate case between the oscillation mode and the mode of slow propagation. $\rho = 6 \cdot 10^6 \text{ml}^{-1}$. Video.

bacteria eat, grow and slowly propagate, for a moment undisturbed by phages. Soon they are met by the expanding phage front after which their growth is stifled. They peak around $1 - 2 \cdot 10^{-3} \mu\text{m}^{-2}$ and all become infected. The balance between bacteria growth and bacteria infection is perfect, so the total amount of bacteria does not change over time.

The front moves fastest in the mode of small ρ, with a constant speed of ≈ 3 mm/h. The propagation speed of the front in the absence of phages is constant in ρ and agrees very well with the bacterial swimming speed observed in [25]. In the intermediate ρ-mode (fig. 27b) the speed oscillates, since the colony swims faster in the periods when bacteria are abundant and thus rapidly consume nutrients.

The transition between the oscillation mode and the mode of slow propagation occurs gradually over a fairly broad range in ρ. In that range, the oscillations seem to become smaller in both wavelength and amplitude. An example of an intermediate case is figure 28b, where the bacterial front progresses slowly in a sliver, as in the third mode, but also wobbles up and down as it progresses, as in the second mode.

Much of this behavior appears to depend strongly on the specific choices regarding nutrient dependence of the model parameters. In the small ρ-mode, bacteria are allowed to deplete nutrients at the front without becoming dense enough that phages can infect them at large scale. This means that all the nutrient dependent parameters (τ_l, β, g_n) take significantly different values a few mm behind the front than they do at the bacterial peak. The same can be said for the oscillatory mode in periods where P is low at the front. In the third mode, in contrast, the bacteria are never permitted to carve out a significant nutrient gradient, and this this comparative spatial homogeneity of the parameters probably plays a role in stabilizing the system in in high-ρ mode.

Introducing lysis inhibition

The same three modes apply to the WT model MS1 with $f_\tau = f_\beta = 2$. Fig. 29 is overall very similar to fig. 27, and comparison between the two does not predict a difference that would be identifiable in the lab.

If f_τ is increased significantly, the extreme modes (bacteria escape or copropagate slowly with infected bacteria) are still accessible at the same ρ-ranges, but the middle mode takes on a different expression (fig. 30). Here, a long tail of LIN'ed bacteria drags behind the front. In fig. 30a this tail is virtually frozen because nutrients were depleted by the bacterial front. In fig. 30b, the tail slowly vanishes, as the remaining nutrients allow bacteria to continually lyse. The expressions in fig. 30 are not achievable in MS0. The difference between fig. 27 and 30 is reminiscent of the difference that was observed between the

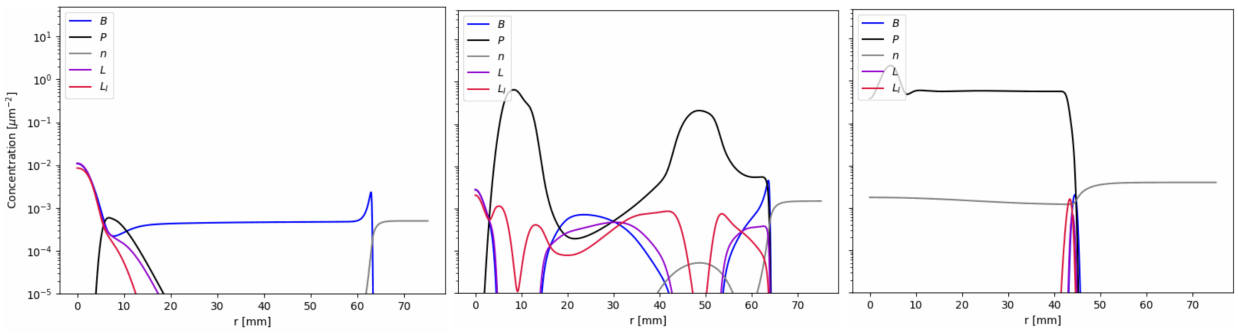

(a) (b) (c)

Figure 29: The three modes of the chemotaxis model for WT T4 (MS1). In all three simulations, $f_\tau = f_\beta = 2$. (a) $\rho = 10^6$ ml^{-1} at $t = 20$ h. Video. (b) $\rho = 3 \cdot 10^6$ ml^{-1} at $t = 30$ h. Video. (c) $\rho = 8 \cdot 10^6$ ml^{-1} at $t = 50$ h. Video.

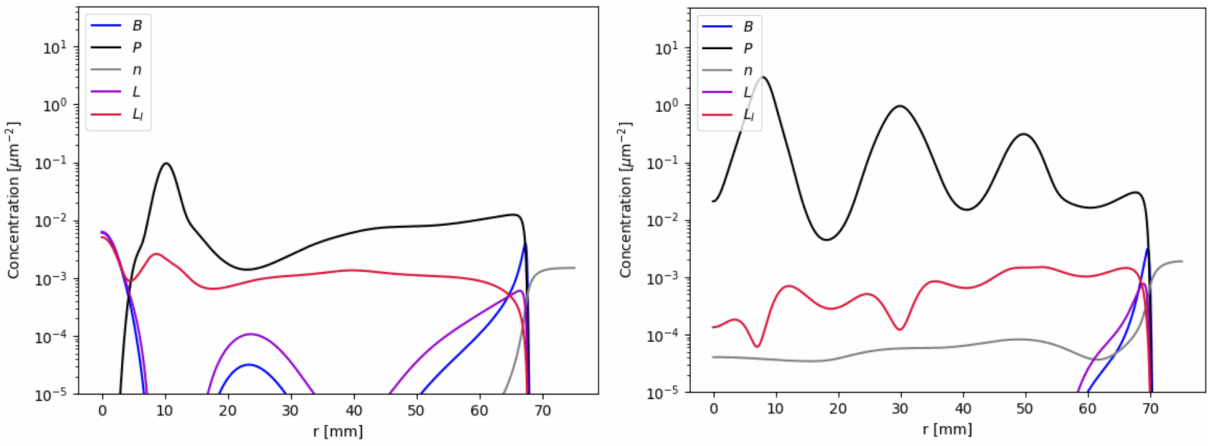

(a) (b)

Figure 30: Results of MS1 with $f_\tau = f_\beta = 10$, $\Delta r = 5\mu$m. (a) $\rho = 3 \cdot 10^6$ml^{-1}, t = 30 h. Video. (b) $\rho = 4 \cdot 10^6$ml^{-1}, t = 40 h. Video.

r-mutant plaque simulation (MP0) and the WT plaque simulation (MP1), in that, in both cases, the phage front spreads at approximately the same speed (compare 27b and 30a) and is followed by a (turbid) region of LIN'ed bacteria in the WT case.

6.5 Discussion of nutrient dependence

Again I need to discuss the nutrient dependence in my models in slightly more detail. Notice in eqs. 1 and 2, as well as the choice of $K_n = n_0/5$, that n_0 (or, equivalently, ρ) is treated as an absolute value that determines how bacteria and phages react to other nutrient concentrations - despite the fact that n_0 is just an experimental parameter. So far, the initial richness of the medium has been fixed between all simulations, and the particular richness that I have selected might in principle happen to be a true absolute reference point of *E. coli* and phage T4. However, in the swimming model, I have decreased the initial richness significantly, because this was necessary to get interesting results, so now I am forced to question this assumption.

I could have chosen instead to define an actual absolute reference point for medium richness and set it, say, equal to the value I have been using so far, ie. $\rho_{ref} = 10^9 \text{ml}^{-1}$. However, this could also be problematic. Deponding on the type of medium, in some cases the decline in growth rate that happens as a culture approaches the carrying capacity is not only due to depletion of nutrients, but also to accumulation of toxic waste products produced by the bacteria themselves. For a bacterium, being inoculated into a medium that has been almost totally depleted of nutrients by bacteria may well "feel" different than being inoculated into one that is just as poor in carbon source, but which is uncontaminated by bacteria. Presumably, the inoculated bacterium will flourish better in the latter situation, even if, in the former situation, one could get the preexisting bacteria to stop consuming any of the remaining nutrients.

The truth is, I don't know of well-tested model that takes these things into account. For a given type of medium, the ideal solution probably lies somewhere between the assumption of an absolute reference concentration and always taking the initial concentration as reference. Nonetheless, for simplicity, I make the latter assumption. Since the initial nutrient concentration turns out to have an enormous impact on the behavior of the swimming model, it would be wise to dig into experimental literature and explore this aspect of the nutrient dependence in my model.

6.6 Discussion of swimming simulations

Once replicable and ordered results exist for T4 in swimming medium, it would be interesting to see whether anything analogous to the modes I observe in MS0 and MS1 is observable in the real-world. For now, I will make a rough and speculative comparison between fig. 23 and my model results, with the caveats that the experimental results are preliminary and not reproducible, and the model results are subject to all the uncertainties I have laid out.

As I mentioned in chapter 2.4, it seems that continued superinfection leads to continued LIN, a nuance that is not considered in my models. This may be an especially problematic omission in the swimming models, in light of the hypothetical scenario sketched out in the introduction to this chapter. If the utility to delaying lysis lies not in postponing for a certain fixed amount of time, but to wait for the cessation of superinfections, which would occur once the host has swum to a new area, then an analysis of the dynamics of LIN in an environment that allows for swimming should take this into account.

The oscillatory mode in MS0 and MS1 was generally characterized by the appearance of spatial waves of bacterial concentration behind the expanding front. Interestingly, some forms of spatial waves are actually observable in the swimming plates in fig. 23. The clearest examples are the smooth and coherent waves in the bottom of fig. 23a. Waves of a slightly different expression can be seen just below the center in fig.

23a. While no actual waves are visible in fig. 23b, it does actually display noisy mm-scale variations in turbidity - evident as a cloudy texture - which may conceivably result from the same temporal oscillations on the expanding front as what is seen in the oscillatory mode for MS0. Even if the r-mutant should lyse all infected cells even when nutrients are depleted, as seems to be the case in plaques, MS0 still predicts some remaining uninfected cells behind the front in the oscillatory mode (fig. 27b). The waves produced in MS0 are generally more on the cm-scale, however (fig. 27). In future experiments, time-lapse monitoring of the plate may provide clues as to how the spatial turbidity variations arise. For instance, it may tell us whether the variations are frozen, or whether some development is still happening after the front has passed.

It is tempting to see a parallel between the large, homogeneous turbid swaths in fig. 23a and the flat red lines in fig. 30. Perhaps, these swaths contain LINed cells, just like the halo in the WT plaque. It would be very interesting to see the result of treating the plate in fig. 23a with chloroform. If that procedure made large areas of the plate transparent, this would make it plausible that a large part of the swimming plate is filled with LINed cells and the WT phage has been able to spread through the plate while keeping many hosts alive. On the other hand, it is possible that the WT phage was simply unable to propagate very far from the inoculation point, and the turbid areas mainly contain uninfected cells. As for fig. 23b, it would be interesting to see a time lapse of that experiment, since I do not know whether the transparent area stretching out to the edge of the plate is an area where cells have been killed by phages, or whether the culture simply never spread that far.

If it is the case that LIN'ed cells have managed to spread to the edge of the plate, and the r-mutant never made it farther than the visibly turbid area, then this may suggest an entirely different mechanism by which a phage may benefit from LIN than the ones considered in chapter 2.4: Perhaps delaying lysis allows the phage to copropagate with the host culture, instead of eradicating it. It may be the case that, non only does LIN not slow down the spread of T4 in a plaque, but it actually allows it to spread farther in a swimming medium, simply because it does not eradicate its host prematurely. This idea would be very interesting to explore in future work on T4 and chemotaxis. Unfortunately, whether or not this mechanism is actually an explanation for the utility of LIN, it does not bear out in MS0 or MS1, as the spreading of the infection is largely unchanged between MS0 and MS1.

7 Conclusion

I have developed models of the dynamics of LIN that are intended to explain and predict macroscopic aspects of systems in which phage T4 - or another lytic phage capable of displaying LIN - interacts with its host. These models ignore one presumably significant aspect of LIN, namely the effect of repeated superinfections. One attempt at addressing this specific question can be seen in appendix B on the alternative model M3. The main purpose of the model is to make a simple representation of the difference between having an inducibly extended lysis time (corresponding to WT) and only being able to perform the rapid lytic cycle (corresponding to an r-mutant). My models can be seen as a first draft - subject to several significant assumptions and simplifications - for a set of models representing this difference.

One of the questions I wished to address in this thesis was, assuming that LIN is an adapted mechanism, why exactly is it useful to extend lysis-time in response to superinfection? Many possible mechanisms can be stated in words, but how do they bear out quantitatively in a model? One prediction of my well-mixed model is that, under certain conditions where WT T4 and an ri-mutant compete for the same bacterial culture, the WT hosts may absorb a significant number of the r-mutants before lysing, and this may contribute significantly to T4 eventually outnumbering the mutant. One might say the WT phage uses its host as bait for competing phages. Concretely, this "sink effect" is expressed as a significant decline in the concentration of free mutant phages in the period between lysis of the mutant's hosts and lysis of the LINed cells. Namiko Mitarai in currently working on reproducing this decline in broth experiments.

My analysis of the plaque model MP has been more focused on characterizing and explaining its relationship to real-world T4 plaques. I have not made a detailed analysis of the results in terms of the utility of LIN, except to state that LIN does not prevent the simulated phage infection from spreading in space, in agreement with experimental results by Abedon. Since the effect of LIN on plaque morphology is distinct, reliable and well-documented, the plaque models MP have been a good way of pressure-testing the general dynamics underlying all the models in this thesis by comparing their predictions to these results. This comparison indicates that my method of representing nutrient dependence of lysis time may be problematic. On one hand, the WT plaque model MP1 reproduces a ring of indefinitely LINed infected cells in a WT plaque, in agreement with experiments by Stephen Abedon. However, MP0 is in disagreement with the same experiments, which suggest that an r-mutant, in contrast to the WT, should leave no infected cells unlysed within the zone of infection, at least within the plaque. One possible way of aligning the plaque models with these results is to use the non-linear nutrient dependence from [19] in τ_l, while keeping the linear dependence in $\tau_{I,l}$. If this method works, it would be interesting to see if it changes the predictions in the well-mixed and swimming models. In future experimental work it would be useful to directly address the question of the effect of nutrient richness, nutrient depletion or growth rate on LIN'ed lysis time.

The swimming models MS are the most complex, and they are also the ones that were developed latest in my thesis period. Most of the time I have spent on these models was dedicated to simply getting meaningful results, and to develop a language to be able to characterize the various types of behavior that the simulations can exhibit. There is much room for deeper analysis of the dynamics of these models, and such analysis could potentially provide very useful information regarding the utility of LIN.

I have shown that MS0 and MS1 exhibit a type of phase transition around $\rho = 3 \cdot 10^6$/ml, below which the bacteria escape phage predation at their maximum swimming speed, and above which phage predation leads to oscillation of the swimming front. This oscillation arises from phages at the front growing rapidly until they suddenly wipe out the majority of the bacteria on the front. Subsequently, the few surviving bacteria escape and swim on, along with the diffusive tail of phages, and the cycle repeats. The oscillations in the oscillatory mode lead to lasting spatial waves in the bacterial density behind the front. In the future it would be very interesting to see replicable results in swimming agar with T4 and to see if they display any similarity to my results. Interestingly, definite coherent waves, as well as more noisy spatial variation

can be seen in the preliminary results in fig 23.

As ρ is increased, the amplitude of these oscillations goes to zero over about a factor of 2 in ρ. Due to the uncertainties in how I model nutrient dependence, which appear to become more and more significant as I increase spatial complexity, I am hesitant to assign much importance to these particular ρ-values.

It is not as easy to determine a winner or loser in the spatial simulations as it was in the well-mixed system. In that system, I could just give the bacteria plenty of nutrients so that growth is only limited by phages, and then count the free phages in the end, since all cells would eventually lyse. In MP and MS, the distribution of nutrients changes significantly in time and space, and many simulations end with significant numbers of infected cells still existing. An attempt to extrapolate from a (simulation of a) lab experiment to nature poses many ambiguities, such as how to weigh "unborn" phages against free phages in an evaluation of how well a phage population has prospered. Though I have not made as clear conclusions about the utility of LIN in the spatial models, I have at least been able to show that LIN does not appear to stifle the spatial propagation of phage T4 because the phages leading the spatial diffusion exist on a tail where phage concentration is low and, consequently, superinfection is unlikely. I have not been able to nail down a solid analytical argument for why this is the case in the plaque model, and I am unsure if it is a totally robust feature of the functional form of the model. I can say that the fact that LIN affects the ZOI by less than $\sim 10\%$ is robust to significant variations in τ_l, β_0 and η.

The swimming models have not led me to a conclusion regarding the effect of LIN on the ability of a phage to spread in space. According the models, LIN has next to no effect on the propagation speed of the bacterial front. As chemotaxis is a defining feature of *E. coli* and its interaction with its environment, the question of the response of a swimming host culture to a T4 phage that can trigger LIN is essential to the question of the evolutionary benefit of LIN. I am excited to see replicable swimming experiments with T4. Apart from providing useful biological information, in and of themselves, such experiments may also be useful in evaluating the validity of the assumptions going into my models.

The use of numerical models in LIN research will aid in both designing and interpreting phage exeriments. I believe a dialectical approach, where simulations motivate experiments, and lab results inform changes to the models, can be a very effective way of establishing a more exact and quantitative understanding of the dynamics underlying phage-bacterium interactions. As a first step, I hope this thesis will lead my supervisor and other researchers to continue the work of applying such an approach to phage T4 and lysis inhibition.

References

[1] M. Zuppi, H. L. Hendrickson, J. M. O'Sullivan, and T. Vatanen, "Phages in the Gut Ecosystem," *Frontiers in Cellular and Infection Microbiology*, vol. 11, 2022.

[2] "Wikipedia: Myoviridae," Jan 2023. [Online; accessed May 12, 2023].

[3] M. R. Clokie, A. D. Millard, A. V. Letarov, and S. Heaphy, "Phages in nature," *Bacteriophage*, vol. 1, pp. 31–45, Jan. 2011.

[4] E. C. Keen, "A Century of Phage Research: Bacteriophages and the Shaping of Modern Biology," *Bioessays*, vol. 37, pp. 6–9, Jan. 2015.

[5] M. Barron, "Phage therapy: Past, present and future," Aug 2022. American Society of Microbiology, www.asm.com.

[6] H. Shuwen and D. Kefeng, "Intestinal phages interact with bacteria and are involved in human diseases," *Gut Microbes*, vol. 14, p. 2113717, Jan. 2022.

[7] S. G. Hays and K. D. Seed, "Dominant Vibrio cholerae phage exhibits lysis inhibition sensitive to disruption by a defensive phage satellite," *bioRxiv*, 2019.

[8] J. D. Karam and E. S. Miller, "Bacteriophage T4 and its relatives," *Virology Journal*, vol. 7, no. 1, p. 293, 2010.

[9] S. Abedon, "Look Who's Talking: T-Even Phage Lysis Inhibition, the Granddaddy of Virus-Virus Intercellular Communication Research," *Viruses*, vol. 11, p. 951, Oct 2019.

[10] Y. Chen and R. Young, "The Last *r* Locus Unveiled: T4 RIII Is a Cytoplasmic Antiholin," *Journal of Bacteriology*, vol. 198, no. 18, pp. 2448–2457, 2016.

[11] J. Filée, F. Tétart, C. A. Suttle, and H. M. Krisch, "Marine T4-type bacteriophages, a ubiquitous component of the dark matter of the biosphere," *Proc. Natl. Acad. Sci. U. S. A.*, vol. 102, pp. 12471–12476, Aug. 2005.

[12] S. Goldin, Y. Hulata, N. Baran, and D. Lindell, "Quantification of T4-Like and T7-Like Cyanophages Using the Polony Method Show They Are Significant Members of the Virioplankton in the North Pacific Subtropical Gyre," *Frontiers in Microbiology*, vol. 11, 2020.

[13] I. V. Krieger, V. Kuznetsov, J.-Y. Chang, J. Zhang, S. H. Moussa, R. F. Young, and J. C. Sacchettini, "The structural basis of T4 phage lysis control: DNA as the signal for lysis inhibition," *J. Mol. Biol.*, vol. 432, pp. 4623–4636, July 2020.

[14] P. Paddison, S. T. Abedon, H. K. Dressman, K. Gailbreath, J. Tracy, E. Mosser, J. Neitzel, B. Guttman, and E. Kutter, "The Roles of the Bacteriophage T4 *r* Genes in Lysis Inhibition and Fine-Structure Genetics: A New Perspective," *Genetics*, vol. 148, pp. 1539–1550, 04 1998.

[15] J. Cahill and R. Young, "Phage Lysis: Multiple Genes for Multiple Barriers," *Adv. Virus Res.*, vol. 103, pp. 33–70, 2019.

[16] B. Gibb, P. Hyman, and C. L. Schneider, "The Many Applications of Engineered Bacteriophages - An Overview," *Pharmaceuticals (Basel)*, vol. 14, p. 634, June 2021.

[17] R. Young, "Bacteriophage lysis: Mechanism and regulation," *Microbiol. Rev.*, vol. 56, pp. 430–481, Sept. 1992.

[18] W. Bode, "Lysis inhibition in *Escherichia coli* infected with bacteriophage T4," *J. Virol.*, vol. 1, pp. 948–955, Oct. 1967.

[19] H. Hadas, M. Einav, I. Fishov, and A. Zaritsky, "Bacteriophage T4 development depends on the physiology of its host *Escherichia coli*," *Microbiology (Reading, England)*, vol. 143 (Pt 1), p. 179–185, 1997.

[20] A. Rabinovitch, I. Fishov, H. Hadas, M. Einav, and A. Zaritsky, "Bacteriophage T4 development in *Escherichia coli* is growth rate dependent," *J. Theor. Biol.*, vol. 216, pp. 1–4, May 2002.

[21] M. Avlund, I. B. Dodd, S. Semsey, K. Sneppen, and S. Krishna, "Why do phage play dice?," *Journal of Virology*, vol. 83, no. 22, pp. 11416–11420, 2009.

[22] M. Wolfram-Schauerte, N. Pozhydaieva, M. Viering, T. Glatter, and K. Höfer, "Integrated Omics Reveal Time-Resolved Insights into T4 Phage Infection of *E. coli* on Proteome and Transcriptome Levels," *Viruses*, vol. 14, p. 2502, Nov 2022.

[23] A. D. Hershey, "Mutation of bacteriophage with respect to type of plaque," *Genetics*, vol. 31, pp. 620–640, Nov. 1946.

[24] "Wikipedia: Erlang distribution," Mar 2023. [Online; accessed May 12, 2023].

[25] D. Ping, T. Wang, D. T. Fraebel, S. Maslov, K. Sneppen, and S. Kuehn, "Hitchhiking, collapse, and contingency in phage infections of migrating bacterial populations," *The ISME Journal*, vol. 14, no. 8, pp. 2007–2018, 2020.

[26] R. S. Eriksen, N. Mitarai, and K. Sneppen, "Sustainability of spatially distributed bacteria-phage systems," *Scientific Reports*, vol. 10, no. 1, p. 3154, 2020.

[27] N. Mitarai, S. Brown, and K. Sneppen, "Population Dynamics of Phage and Bacteria in Spatially Structured Habitats Using Phage λ; and *Escherichia coli*," *Journal of Bacteriology*, vol. 198, no. 12, pp. 1783–1793, 2016.

[28] M. De Paepe and F. Taddei, "Viruses' Life History: Towards a Mechanistic Basis of a Trade-Off between Survival and Reproduction among Phages," *PLOS Biology*, vol. 4, 06 2006.

[29] Z. J. Storms, E. Arsenault, D. Sauvageau, and D. G. Cooper, "Bacteriophage adsorption efficiency and its effect on amplification," *Bioprocess and biosystems engineering*, vol. 33(7), pp. 823–831, 2010.

[30] J. Hu, K. Miyanaga, and Y. Tanji, "Diffusion of bacteriophages through artificial biofilm models," *Biotechnology progress*, vol. 28, pp. 319–26, 03 2012.

[31] N. I. Østerlund, "Spatiotemporal dynamics and interaction of m13phage with its satellite phage," Master's thesis, University of Copenhagen, 2018.

[32] A. L. Koch, "The growth of viral plaques during the enlargement phase," *Journal of Theoretical Biology*, vol. 6, no. 3, pp. 413–431, 1964.

[33] S. Chatterjee, R. A. da Silveira, and Y. Kafri, "Chemotaxis when Bacteria Remember: Drift versus Diffusion," *PLoS Computational Biology*, vol. 7, p. e1002283, Dec. 2011.

[34] U. Alon, M. G. Surette, N. Barkai, and S. Leibler, "Robustness in bacterial chemotaxis," *Nature*, vol. 397, pp. 168–171, Jan. 1999.

[35] T. Jakuszeit, J. Lindsey-Jones, F. J. Peaudecerf, and O. A. Croze, "Migration and accumulation of bacteria with chemotaxis and chemokinesis," *The European Physical Journal E*, vol. 44, no. 3, p. 32, 2021.

[36] X. Li, F. Gonzalez, N. Esteves, B. E. Scharf, and J. Chen, "Formation of phage lysis patterns and implications on co-propagation of phages and motile host bacteria," *PLOS Computational Biology*, vol. 16, pp. 1–22, 03 2020.

[37] J. B. Kirkegaard, "A Brief Introduction to Numerical Methods in Physics," 2021.

[38] B. R. Levin, F. M. Stewart, and L. Chao, "Resource-Limited Growth, Competition, and Predation: A Model and Experimental Studies with Bacteria and Bacteriophage," *The American Naturalist*, vol. 111, no. 977, pp. 3–24, 1977.

[39] S. H. Strogatz, *Nonlinear Dynamics and Chaos: With Applications to Physics, Biology, Chemistry and Engineering*. Perseus Books Group, 2015.

Appendices

A Supplementary material - Animations and source code

Animation url's

Fig. 18a - https://vimeo.com/827652183?share=copy
Fig. 18b - https://vimeo.com/827658747?share=copy
Fig. 26 - https://vimeo.com/828009210?share=copy
Fig. 27a - https://vimeo.com/827658946?share=copy
Fig. 27b - https://vimeo.com/827659153?share=copy
Fig. 27c - https://vimeo.com/827659269?share=copy
Fig. 28b - https://vimeo.com/828014940?share=copy
Fig. 29a - https://vimeo.com/827659376?share=copy
Fig. 29b - https://vimeo.com/827659544?share=copy
Fig. 29c - https://vimeo.com/827659651?share=copy
Fig. 30a - https://vimeo.com/827659757?share=copy
Fig. 30b - https://vimeo.com/827659852?share=copy

Source code

https://github.com/UlrikHvid/Masters-thesis

B M3 - Increasing burst size for extended lysis inhibition

M1 is simple, but it lacks some features that may be key to the evolutionary significance of LIN. In the real world, it probably matters not just *whether* you get superinfected, but also how many times and when. Lysis can, as far as is known, be postponed indefinitely in this way [15]. In addition, a cell that stays in the inhibited state for an extended amount of time due to continual superinfections, will keep producing more progeny, leading to a burst size that increases with the time that it was inhibited. Without these properties, which are not included in M1, the fitness benefit of LIN is likely much smaller, since in M1 the sensitivity to the phage concentration in the environment disappears after the second infection, and since the great advantage of an extended LIN, namely a far greater burst size, is not included.

In order to include these properties of LIN, I have written a model where I make $M \cdot N$ infected states, denoted by $L_{i,j}$ where $i \in [1, M]$ is the number of infections and $j \in [1, N]$ is the index of the progression substate that the cell is in. A cell in state $L_{i,j}, j < N$ progresses to state $L_{i,j+1}$ with rate $1/\tau(n)$ with τ understood in the same way as in the previous models. A cell in state $L_{i,N}$ can lyse with rate $1/\tau(n)$ and with burst size $i \cdot \beta(n)$, ie. burst size increases linearly with *number of infections*. In a sense, number of infections comes to represent time, since the natural assumption is that burst size will increase linearly with time. Superinfection takes $L_{i,j} \to L_{i+1,1}$ unless $i = M$ in which case $L_{M,j} \to L_{M,1}$. This latter rule implies that, even though lysis inhibition can be extended indefinitely, there is a limit to the number of phages that a cell can contain. A cell in $L_{M,1}$ is unaffected by superinfection.

The fact that number of superinfections becomes a heuristic for time could be problematic. In a situation with a high concentration of phages, cells will move very quickly through the superinfection indices, corresponding to phages being generated at an enormous rate. However, in this situation, phages will also be kept for a very long time in the final state, which does add extra time before lysis, and in many cases the result may be the same: the cell takes a very long time to lyse, and it produces the maximum number of phages.

In addition to eqs. 5 and 10, M3 is constituted by the following ODE's.

$$\frac{\mathrm{d}L_{1,1}}{\mathrm{d}t} = \underbrace{\eta\, P\, B}_{\text{infection}} - \underbrace{\eta\, P\, L_{1,1}}_{\text{superinfection}} - \underbrace{L_{1,1}/\tau(n)}_{\text{state progression}} \tag{76}$$

$$\frac{\mathrm{d}L_{i,1}}{\mathrm{d}t} = \underbrace{\eta\, P \sum_{j=1}^{N} L_{i-1,j}}_{\text{superinfection}} - \underbrace{L_{i,1}/\tau(n)}_{\text{state progression}} \quad i \in [2, M-1] \tag{77}$$

$$\frac{\mathrm{d}L_{M,1}}{\mathrm{d}t} = \underbrace{\eta\, P \left(L_{M-1,1} + \sum_{j=2}^{N} (L_{M-1,j} + L_{M,j}) \right)}_{\text{superinfection}} - \underbrace{L_{M,1}/\tau(n)}_{\text{state progression}} \tag{78}$$

$$\frac{\mathrm{d}L_{i,j}}{\mathrm{d}t} = \underbrace{(L_{i,j-1} - L_{i,j})/\tau(n)}_{\text{state progression}} - \underbrace{\eta\, P\, L_{i,j}}_{\text{superinfection}}\ ,\ i \in [1, M], j \in [2, N-1] \tag{79}$$

$$\frac{\mathrm{d}L_{i,N}}{\mathrm{d}t} = \underbrace{L_{i,N-1}/\tau(n)}_{\text{state progression}} - \underbrace{\eta\, P\, L_{i,N}}_{\text{superinfection}} - \underbrace{L_{i,N}/\tau(n)}_{\text{lysis}}, i \in [1, M] \tag{80}$$

$$\frac{\mathrm{d}P}{\mathrm{d}t} = \underbrace{\frac{1}{\tau(n)} \sum_{i=1}^{M} i \cdot \beta(n)\, L_{i,N}}_{\text{lysis}} - \underbrace{\eta\, P\, B_{tot}}_{\text{infection}} \tag{81}$$

$$\text{with } B_{tot} \equiv B + \textstyle\sum_{i,j=1}^{N,M} L_{i,j} \tag{82}$$

C Chemostat and linear stability analysis

M0, M1 and M3 represent systems that contain a certain amount of nutrition which is depleted over time. However, I also want to explore the possibility of steady states in a system where there is a continuous inflow of nutrition. So for each mode, I introduce an extra parameter, α, the depletion rate. Each variable gets an extra term, $\frac{\mathrm{d}y}{\mathrm{d}t} = ... - \alpha y$ (each particle in the system has some probability of being expelled in a given time interval) and the nutrition equation gets an extra term $+\alpha n_0$ (constant inflow of nutrients). α is an experimental parameter, and the only requirement is that it must be smaller than the growth rate by some margin, otherwise the bacteria concentration goes to zero. Below, I use the chemostat versions of the models. Note, the results presented in this appendix were made at an early stage and the use a different value of η than the one given in table 1. In this chapter, $\eta = 10^{-9}$. The qualitative conclusions regarding stable oscillations and monotonically increased instability from M0 to M1 to M3 are robust to this change in η.

Figure 31 shows an example run for M0. With these fairly arbitrary initial values, the system immediately starts oscillating with increasing amplitude. All infected states oscillate in sync but are shifted slightly from each other. Except for periods of sharp decrease, L_1 and the concentration decreases as you go up through higher infection states L_i.

The system immediately starts oscillating with increasing amplitude, and it is clear that if there is a stable fixed point, the system will tend to overshoot it with increasing speed, when coming from far away. If I run the model for longer than shown in figure 31, the system eventually jumps back up with such a large slope, that the computation time for *solve_ivp* diverges during the rebound. Having seen the same result using several of the numerical methods included in *solve_ivp*, including the stiff method "LSODA", I believe that this violent rebound is a true effect of the model and not the result of numerical error. These violent oscillations are clearly unbiological, and in terms of biology, we can safely disregard anything that happens after the concentration of bacteria has reached a concentration on the order of 1 ml^{-1}, since in a real scenario this would represent extinction of the colony.

In terms of the model, it is likely that the system converges on stable, if extreme, oscillations, though I cannot show this, since the integration algorithm crashes. However, if I run a simpler version of the model, with only $N = 2$ infected states, then the algorithm can keep up, and it does indeed show stable oscillations (figure 32). This makes it reasonable to assume that the true solution would also be stable oscillations for $N = 10$.

Running M1 and M3 with $f_\tau = f_\beta = 2$, we see that they also predict collapse of the bacterial colony (figure 33). At first glance, including lysis inhibition seems to make the system even more unstable, with the effect being most pronounced in M3.

In the beginning of the simulation seen in figure 33b, the concentration of the substates $L_{i,j}$ seems to decrease approximately exponentially with i, the number of infections. This is good, because it means that the rather arbitrary choice of discounting MOI's of more than 10 has a vanishing effect on the model. However, during and after the collapse of the bacterial colony around $t = 1000$, the phages come to dominate everything, along with $L_{10,j}$, which presumably means the average MOI grows to much higher than 10. At this point, M3 becomes harder to interpret. This may not be a problem however because, as I will discuss later, the collapse of the bacterial colony already constitutes a divergence from experimental outcomes.

It has been noted before that 0D Lotka-Volterra type models of bacteria-phage interactions predict a collapse of the bacterial colony which contrasts real-world experiments [26], [38]. This could attest to - among other things - the invalidity of the well-mixed assumption in a real-world microbial system, even one as well-ordered as a chemostat. Models have been developed which take spatial heterogeneity into account in a way that allows for coexistence of bacteria and phages in the long term. One example by Eriksen et al. [26] used a 3D lattice model to simulate the bacterial microcolonies distributed in space.

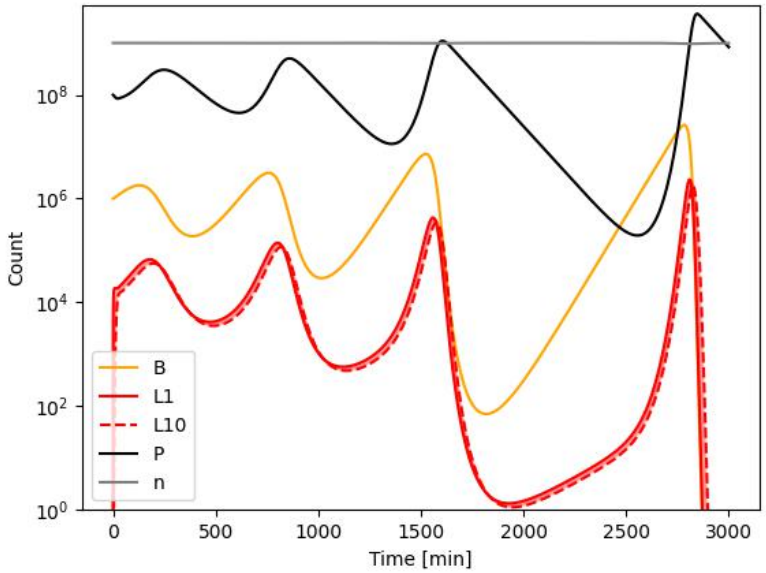

Figure 31: Example run of M0 with default parameters and initial values. Intermediate infection states are represented by transparent curves that lie between those of L_1 and L_{10}.

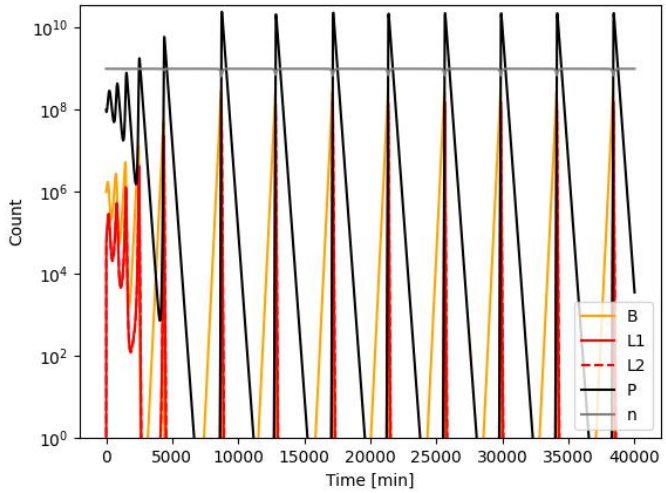

Figure 32: With $N = 2$, M0 converges to stable oscillations.

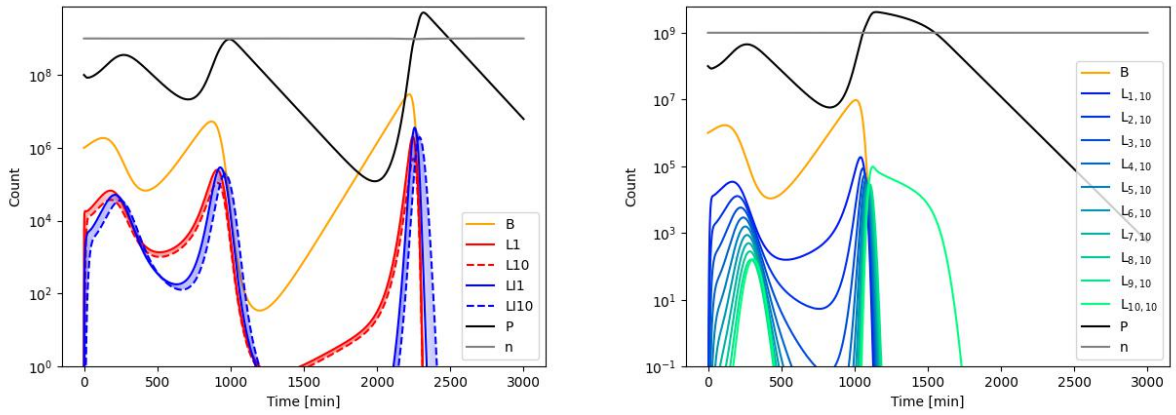

(a) M1

(b) M3

Figure 33: Example runs of M1 and M3 with default parameters and initial values. For M1, all variables are plotted. For M3, which has 103 variables, I only plot states that are about to burst.

In this model, bacteria inside a microcolony are shielded from infection by free phages and can only be infected once a neighboring bacterium lyses.

Linear stability analysis

To examine the effect of LIN on the stability of a chemostat system more rigorously, I perform linear stability analysis (as presented in Strogatz, [39]) on the models. All the necessary calculations are done numerically using the optimize and linalg modules under scipy. The steady state is found using *fsolve*, the jacobian is found using *approx_fprime* and the eigenvalues/vectors are found with *eig*.

M0

With the default parameters, the steady state for M0 is approximately (in units ml^{-1}) $B = 8.21 \cdot 10^5, L_i \approx 2 \cdot 10^4, P = 1.5 \cdot 10^8$. The jacobian for this steady state has two (mutually complex conjugate) eigenvalues with positive real part: $\lambda = 0.00109 \pm 0.0111i$ min^{-1}, with the corresponding eigenvector pointing straight along the P-axis. This indicates that the steady state is unstable and will lead to oscillations. This is indeed what we see when running the simulation with the steady state as initial condition (figure 34). The steady state appears stable on a timescale much longer than $\tau_0 = 20\mathrm{min}$, but eventually we see that the system starts oscillating with exponentially increasing amplitude, as the positive eigenvalue would suggest. I will refer henceforth to the real part of the mode with which has the highest real part as the *instability* of the system, and I will calculate the period of the steady state as $2\pi/Im(\lambda)$.

Since the default parameters are round numbers, lying somewhere in the fairly large area of parameter space spanned by the experimental literature, it is worth asking to what extent the instability of the system depends on the model parameters. Would a small change to the parameters make the system stable?

Figure 35 implies, that the answer is no. Disregarding the very lowest values used for β, the stability of the steady state is independent of β. The same is true for the period of the oscillation around the fixed point. The lowest value used is 10% of the default value, ie. $\beta = 15$, so well outside the spectrum for T4.

Both instability and period increase with τ. Specifically, the period increases linearly with τ (figure 36b), with a slope of ≈ 3. The instability also increases monotonously, but with decreasing slope. Smallest value used for τ is 0.1% of the default value, and it leads to a tiny negative value.

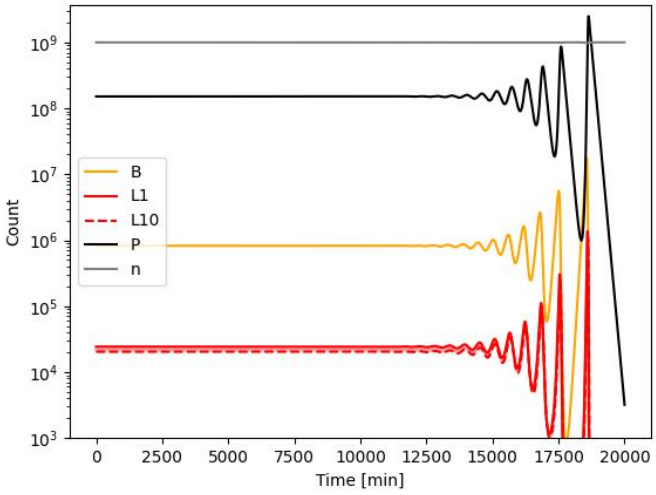

Figure 34: M0 has a steady state which appears stable for many lytic cycles but which eventually starts to oscillate wildly.

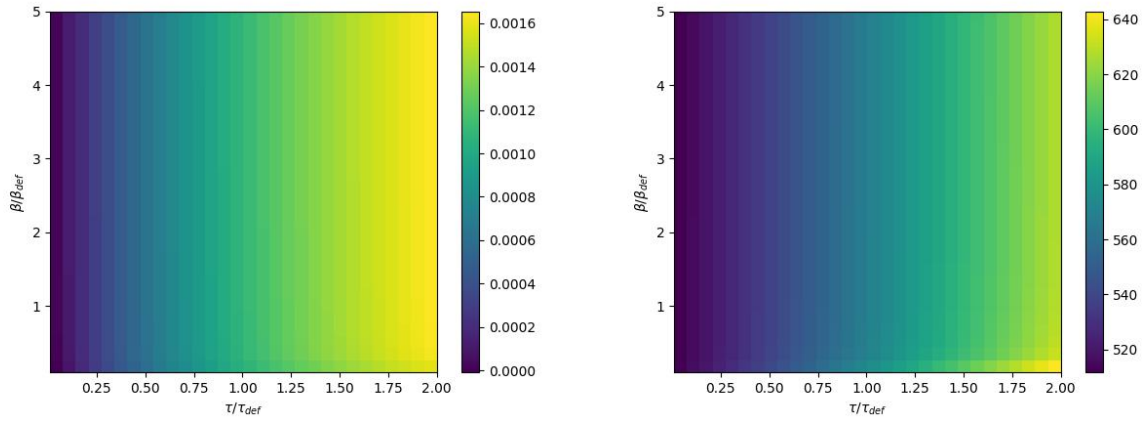

(a) (b)

Figure 35: (a) Instability of most unstable mode. Specifically, the largest real component of the jacobian eigenvalues. (b) Period of the most unstable mode, given by $2\pi/\mathrm{Im}(\lambda)$.

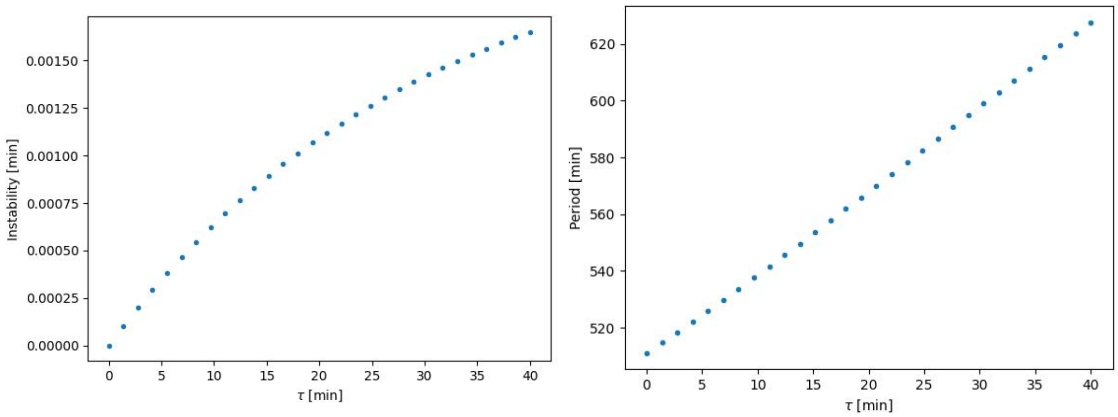

(a) (b)

Figure 36: M0. Instability (a) and period (b) of unstable mode plotted over lysis time. All other parameters set to default value.

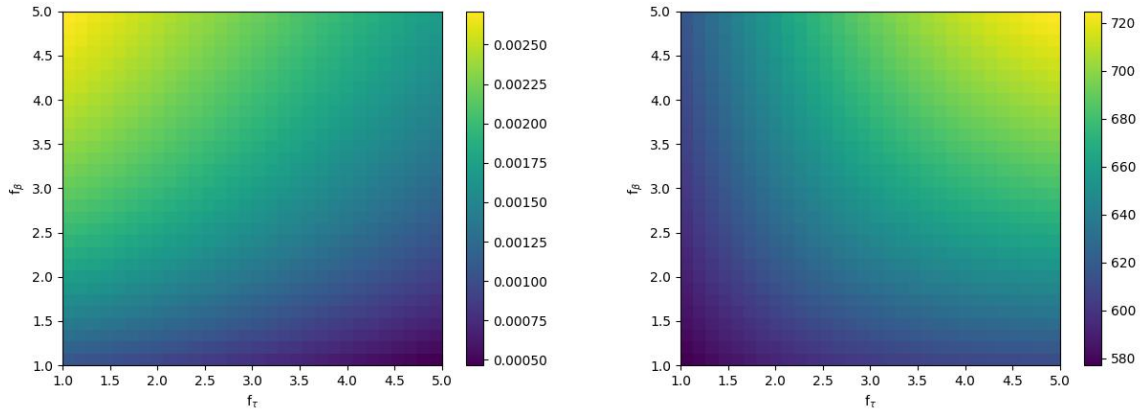

(a) (b)

Figure 37: Properties of the steady state of M1 as function of the LIN parameters f_τ and f_β. (a) Instability. Units are min^{-1}. (b) Period. Units are min.

Taken together, figures 36a and 36b tell us that the limit of $\tau \to 0$ (immediate lysis) leads to a stable steady state with damped oscillations of a period of ≈ 510 min. As we crank up the lysis time, we get a linear increase in the period. Some $\tau_c \ll 20$ min constitutes a Hopf bifurcation [39], a critical value, below which the system approaches the steady state in damped oscillations, but above which the steady state is unstable and leads to oscillations within some limit cycle.

M1 and M3

So what is the effect of lysis inhibition of the stability of the system? For default parameters, the steady state jacobian of M1 has two unstable modes, pointing along the P-axis, with $\lambda = 0.0016 \pm 0.010\, i$. So, for the default parameters, the instability has been increased slightly, but not drastically, as can be confirmed by running the simulation from the steady state.

Varying the LIN parameters f_β and f_τ, I get the eigenvalues shown in figure 37. The resulting shapes look different from those of figure 35, with the direction of steepest ascent for instability pointing towards

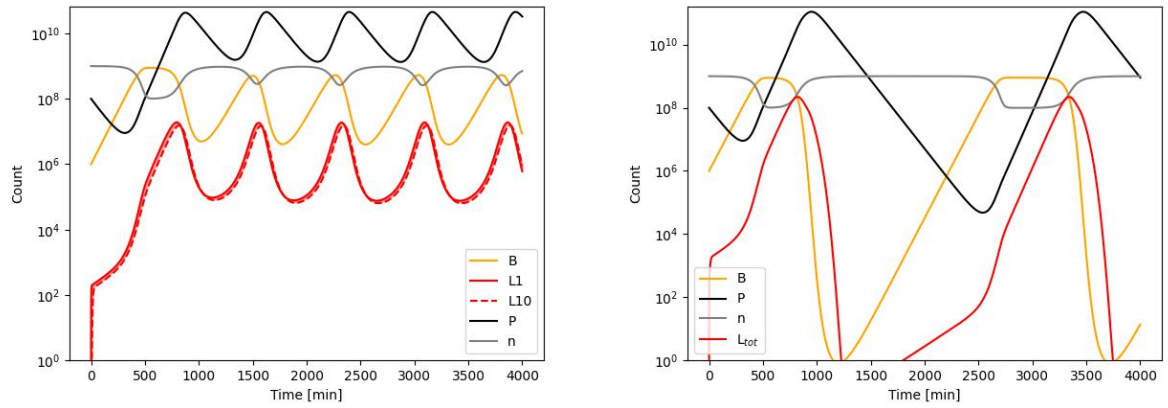

(a) (b)

Figure 38: M0 (a) and M3 (b) with $\eta = \eta_{def}/100$. For a phage with much smaller adsorption rate, the LIN-deficient version shows reasonable steady oscillations, whereas the LIN version has so violent oscillations, that it corresponds to extinction.

increasing f_{beta} and decreasing f_{tau}. The oscillation period increases with both parameters. The area in the lower right corner of fig. 35a has lower instability than M0, indicating that, in pure modeling terms, LIN can have both a stabilizing and destabilizing effect. But, as the testruns had indicated, for parameters describing T4, LIN seems to have a destabilizing effect.

The steady state of M3 has unstable modes with $\lambda = 0.0021 \pm 0.010\ i$, using default parameters. Here, introducing lysis inhibition has doubled the real value of the unstable modes. This confirms again the suspicion from the testruns, that a model that allows the phage to inhibit lysis indefinitely, occasionally increasing burst size by large factors, amplifies the tendency of the Lotka-Volterra-style model to drive the bacterium to extinction.

Note that in the steady state, the variables $L_{i,j}$ decrease exponentially with the number of infections, i. For $i > 7$, the concentrations are one the order of $1\mathrm{ml}^{-1}$ or less. This suggests that the cap I have put on burst size through the variable $M = 10$ is large enough not to have a significant effect on a coexistence state between phages and bacteria. If we make the phages much less virulent, for instance by decreasing η by to orders of magnitude, the dynamical difference between including and omitting LIN becomes more pronounced.